IZMIR KATIP CELEBI UNIVERSITY

GRADUATE SCHOOL OF NATURAL AND APPLIED SCIENCES

CUSTOM DESIGNED OPTICAL TWEEZER FOR TRAPPING YEAST CELLS

M.Sc. THESIS

Nur ÇOBANOĞLU

Department of Nanoscience and Nanotechnology

Thesis Advisor: Assist. Prof. Aziz KOLKIRAN

JANUARY 2018

IZMIR KATIP CELEBI UNIVERSITY
GRADUATE SCHOOL OF NATURAL AND APPLIED SCIENCES

CUSTOM DESIGNED OPTICAL TWEEZER FOR TRAPPING YEAST CELLS

M.Sc. THESIS

Nur ÇOBANOĞLU
(Y150203004)

Department of Nanoscience and Nanotechnology

Thesis Advisor: Assist. Prof. Aziz KOLKIRAN

JANUARY 2018

İZMİR KÂTİP ÇELEBİ ÜNİVERSİTESİ
FEN BİLİMLERİ ENSTİTÜSÜ

ÖZEL YAPIM OPTİK CIMBIZ İLE MAYA HÜCRESİ MANİPÜLASYONU

YÜKSEK LİSANS TEZİ

Nur ÇOBANOĞLU
(Y150203004)

Nanobilim ve Nanoteknoloji Anabilim Dalı

Tez Danışmanı: Yrd. Doç. Dr. Aziz Kolkıran

OCAK 2018

Nur ÇOBANOĞLU, a **M.Sc.** student of **IKCU Graduate School Of Natural And Applied Sciences**, successfully defended the thesis entitled **"CUSTOM DESIGNED OPTICAL TWEEZER FOR TRAPPING YEAST CELLS"**, which she prepared after fulfilling the requirements specified in the associated legislations, before the jury whose signatures are below.

Thesis Advisor :   **Assist. Prof. Aziz KOLKIRAN**   ....
Izmir Katip Celebi University

Jury Members :   **Assist. Prof. Aziz KOLKIRAN**   ....
Izmir Katip Celebi University

Assoc. Prof. Mustafa CAN   ....
Izmir Katip Celebi University

Prof. Dr. Muzaffer ADAK   ....
Pamukkale University

Date of Submission : 12.12.2017
Date of Defense   : 05.01.2018

To my family,

FOREWORD

This thesis is my final work for completion of master degree at Department of Nanoscience and Nanotechnology in Izmir Katip Celebi University. The goal of the thesis is the development of custom designed optical tweezer in order to trap yeast cells and study the possibility of optical tweezer in biological applications. From beginning to end, all steps of this thesis were under the supervision of Assist. Prof. Aziz Kolkıran.

Firstly, I am grateful to my supervisor, Assist. Prof. Aziz Kolkıran, for his excellent guidiance, valuable and constructive suggestions during my master degree.

In addition, I would like to thank to Erdal Kurt for his supports during my thesis.

Finally, I would like to thank my parents, Uğur Çobanoğlu and Nurdan Çobanoglu, and my brother, Can Çobanoğlu, for supporting me and being a source of motivation and inspiration in my life.

December 2017   Nur ÇOBANOĞLU

x

TABLE OF CONTENTS

ABBREVIATIONS

FWHM   **:** Full Width Half Maximum
GLMT   **:** Generalized Lorenz-Mie Theory
NA   **:** Numerical Aperture
R   **:** Reflection
T   **:** Transmission
TE   **:** Transverse Electric
TM   **:** Transverse Magnetic

SYMBOLS

a	: Radius of the bead
a_n, b_n	: Wave scattering amplitudes
A_n^m, B_n^m	: Partial wave scattering amplitudes
$\mathbf{B}$	: Magnetic field
c	: Speed of light
C_n^m, D_n^m	: Partial wave interior amplitudes
$\mathbf{D}$	: Diameter
d_{obj}	: Incident beam diameter to objective
$\mathbf{E}$	: Electric field
E_0	: The peak electric field strength
f_c	: Corner frequency
F_g, F_s, F_T	: Beam confinement parameter
$f/\#$	: Photographic f number
$g_{n,TE}^m, g_{n,TM}^m$	: Beam shape ccoefficients
$\mathbf{H}$	: Kinetic energy
$\mathbf{I}$	: Intensity of the light
k, k_x, k_y	: Stifnesses
k_b	: Boltzmann's constant
$\mathbf{N}$	: Number of frames
n_p, n_{md}	: Refractive indexes
$\hat{n}$	: Normal to surface
$\mathbf{P}$	: Power
$P_n^{|m|}$	: Legendre function
$\mathbf{Q}$	: Trapping efficiency
q_1, q_2	: Parameters of Gaussian beam before and after the optical element
r	: Position of the beam
R	: Fresnel reflection coefficient
$R(z)$	: Radius of curvature
s	: Beam confinement parameter
T	: Fresnel transmission coefficient
u_x, u_y	: Broomwich potentials
v	: Velocity
w_0	: Electric field half-width
w_0	: Beam waist diameter
$w(z)$	: Radius of the beam
ω_{trap}	: Trap depth
x	: Distance of the bead's center from trap center
z_R	: Rayleigh range
λ	: Wavelength

$\boldsymbol{\psi_n}$ **:** Ricatti-Bessel function
$\boldsymbol{\theta}$ **:** Incident ray angle
$\boldsymbol{\varphi}$ **:** Refracted ray angle
ζ_n **:** Ricatti-Henkel functions
$\boldsymbol{\mu}$ **:** Viscosity of the medium
γ **:** Drag coefficient
τ **:** Time constant
$<x^2>$ **:** Time-averaged square of the bead's horizontal displacement from the center of the trap.
$<y^2>$ **:** Time-averaged square of the bead's vertical displacement from the center of the trap.

LIST OF TABLES

LIST OF FIGURES

CUSTOM DESIGNED OPTICAL TWEEZER FOR TRAPPING YEAST CELLS

ABSTRACT

The goal of this study is developing custom designed optical tweezer which uses two He-Ne lasers (λ=632.8 nm) parallel to each other to trap yeast cells. The characteristic specs of this optical tweezer determined by Brownian Motion of polystyrene beads in water. Stiffness and trapping forces of optical tweezer calculated for laser 1, laser 2 and when both lasers used simultaneously. Laser 2 can trap and move particle to laser 1 and multiple particles can be trapped by the laser 1. After determination of specs of optical tweezer, yeast cells in yogurt culture medium were trapped by laser 1 and laser 2. Stiffness of optical tweezer and trapping force on yeast cells were determined by drag force and Brownian motion methods by assuming the medium was homogenous and had viscosity of 0.038 kg/ms. Viscosity depends on the concentration of fluid and surface. Viscosity of the yogurt culture medium which was used in experiments was calculated theoretically with respect to velocity of fluid and specs of optical tweezer calculated previously. Possibility of application inside yeast cells was studied theoretically by using viscosity of cytoplasmic medium. As a result of this study, this custom designed optical tweezer which uses two He-Ne lasers are applicable in life sciences like inside cells, viscosity measurements and drug delivery systems.

ÖZEL YAPIM OPTİK CIMBIZ İLE MAYA HÜCRESİ MANİPÜLASYONU

ÖZET

Bu çalışmanın amacı maya hücrelerini yakalamak için iki adet birbirine paralel He-Ne lazer (λ=632.8 nm) kullanan özel yapım optik cımbız geliştirmektir. Bu optik cımbızın karakteristik özellikleri su içerisindeki polisitiren küreciklerinin Brownian hareketleriyle belirlenmiştir. Optik cımbızın sertliği ve yakalama kuvvetleri lazer 1, lazer 2 ve her iki lazerin aynı anda kullanıldığı zaman için hesaplanmıştır. Lazer 2 parçacıkları yakalayıp lazer 1'e taşıyabilmektedir ve birden fazla parçacık lazer 2 tarafından yakalanabilmektedir. Optik cımbızın özellikleri tanımlandıktan sonra yoğurt kültürü içindeki maya hücreleri lazer 1 ve lazer 2 tarafından yakalanmıştır. Optik cımbızın sertliği ve maya hücreleri üzerindeki yakalama kuvveti ortamın homojen ve viskozitesinin 0.038 kg/ms olduğunu kabul ederek Brownian hareketi ve sürüklenme kuvveti methodlarıyla belirlenmiştir. Viskozite konsantrasyona ve yüzeye bağlı olarak değişmektedir. Deneylerde kullanılan yoğurt kültürünün viskozitesi akışkanın hızına ve optik cımbızın özelliklerine göre teorik olarak hesaplanmıştır. Hücre içinde uygulanma ihtimali için hücre sitoplazmasının viskozitesi kullanılarak teorik olarak çalışılmıştır. Bu çalışmanın sonucu olarak; bu 2 adet He-Ne lazer kullanan özel yapım optik cımbız; hücre içinde, viskozite ölçümleri ve ilaç taşınımı gibi fen bilimleri uygulamalarında kullanılabilmektedir.

1. INTRODUCTION

Optical tweezers are defined as the highly focused laser beams which can trap and manipulate the particles between nanometer and micrometer size range by means of radiation pressure. In 1970, Ashkin was reported that particles were accelerated by radiation pressure [1]. In 1986, For optical trapping of dielectric particles, single highly focused laser beam was developed by focusing laser beam into high numerical aperture objective [2]. They have been used in biological applications such as molecular motors studies, single molecule experiments and cellular manipulation since 1987 when Ashkin and Dziedzic trap bacteria and viruses by using green laser [3,4]. Instead of just a manipulation of particles, optical tweezers can be used to control or measure the forces on biological processes[5].

The trapping mechanism is the result of the exchange of momentum between trapping light and trapped particle. Resulting force occurs due to momentum exchange and depends on the size of particle: Ray optics approximation, Rayleigh approximation and Generalized Lorenz-Mie Theory.

The gradient force and the scattering force form the net force on the particle. Scattering force pushes the particle in the direction of beam propagation whereas gradient force pulls the particle towards the higher internsity regions. Stable trapping can be achieved when the gradient force is greater than the scattering force [5,6].

Assuming that trapping potential is harmonic and trapping force can be characterized by several calibration methods. Force can be calculated by the measuring the displacement of the beam from the trap center and fluid velocity. This force is the drag force and it is assumed that drag force equals to trapping force. Another way of measuring the trap force is Brownian Motion Method. In Brownian Motion Method, trap stiffness can be determined without any information about viscosity of fluid and geometry of particle [7,8].

1.1 Historical Background of Optical Tweezers

Optical tweezers demonstrate that light is able to exert a force on matter. Quantum theory states the momentum carried per photon. Prior to quantum mechanics, it is predicted that there exist "radiation pressure" as a result of electromagnetic theory developed by James Clerk Maxwell [9]. It describes that there is a pressure in the direction normal to the wave in a medium where the waves are propagated and it numerically equals to the energy contained in unit volume [10].

Bartoli predicted such pressure in thermodynamic context which is called as Maxwell-Bartoli force [11] and Crooks discovered the radiometric forces [12]. Two papers published by P.N. Lebedew and by E. F. Nichols and G. F. Hull in 1901. Papers had independent results but same approximation to study the effect of the light, produced by an arc lamp, had on thin vanes. Low gas pressures and thin metallic vanes were used by Lebedew on the contrary high pressure gas and silvered glass vanes used by Nichols and Hull [13,14]. In second paper, measurements were carried out for providing the validation of results of Nichols and Hulls in the high pressure limit since the gas could be neglected over short exposures of the vanes to the light [15]. Nichols and Hulls analysed the experiments in accordance with their historical backgrounds and compared them. As a conclusion, they found that both experiments had measurement errors but both qualitatively proved the existence of the radiation pressure without quantitatively following the theory of Maxwell-Bartoli forces. In 1903, Nichols and Hull published the quantitative demonstration [15].

Studies of optical manipulation began by Arthur Ashkin in 1970s. Although discovery of lasers has provided convenience to study optical forces due to much higher intensities of lasers, optical forces are dominated by radiometric forces and it is too difficult to observe their direct effects. Ashkin could observe the radiation pressure due to reflection from such particles by using transparent particle and transparent medium while avoiding heating problems. In 1970, he found that particles were trapped by the laser beam and travelled in the direction of beam propagation [1]. He has demonstrated that gradient force is created by intensity gradient of the laser beam, pulls the high-refractive-index particles toward the beam axis and push low-refractive-index particles away from the axis. He hypothesized

that light could rotate and accelerate the particles. He also discussed about magneto-optical trap and atomic dipole trap. By using two beams which propagates against each other, an optical trap can be created where particles are under influence of a combination of gradient force and radiation pressure [10].

The next year, Ashkin and J. M. Dziedzic as a co-author trapped glass beads suspended in air by single laser beam which was directed upward so that the radiation pressure balances the gravitational force on the particle. They observed that if the beam was turned off after dragging, the bead was allowed to go back to equilibrium position without oscillation. Moreover, they said that laser modes different from the normal TEM_{00} Gaussian beam, such as TEM_{01} and TEM_{01*}, a doughnut mode could be used [16]. Ashkin also found that this new technique was possible in high vacuum and for stabilizing particle position by using feedback mechanism [10,17,18]. He observed new types of nonlinear effects and studied the effect of radiation pressure on a liquid interface [19,20].

In 1970s, optical levitation of droplets was studied most as application of optical manipulation. Ashkin and Dziedzic studied how both solid and liquid airborne particles can be trapped and the ways of carrying types of experiments such as crystallization and simple measurements on particle interactions. This paper also shows problems due to optical levitation, such as trapping multiple particles but not controlling them independently [21].

Ashkin and Dziedzic show how to make sensitive measurements on levitated droplets by stabilization method [22]. In this paper, they studied effects of wavelength and size on variations of optical forces. Size determination was provided highly sensitive by the resonances excited within the droplets. This technique is commonly used for size measurement now, and it can be combined with other techniques such as Raman spectroscopy [23], to determine the size and composition of particle.

In 1986, Ashkin, Dziedzic, Bjorkholm, and Chu studied trapping with single beam laser focusing through high numerical aperture (NA) microscope objective. By this way, the particle could be trapped in the plane transverse to the laser beam propagation and in the axial direction. Therefore, the particles could be trapped by

beam directed downward and they were held against gravity. They demonstrated a tweezer which has second beam to guide particles into trapping region. Tweezer was able to trap particles between 25 nm and 10 μm [2].

They open new size regime to optical trapping by optical tweezers. Ashkin and Dziedzic were the first ones who trap bacteria and viruses by optical tweezers which used green laser [3]. Green laser has disadvantages on trapping biological samples since biological samples absorbs strongly green laser therefore they are easily damaged. In 1987, Ashkin and his collegues overcomed this problem by using infrared laser to trap cells without damaging. The usage of infrared beams is important for biological experiments, in almost all biological experiments such wavelengths are used.

1.2 Applications of Optical Tweezers

New viewpoints in microscopic world to manipulation of small objects have been created by trapping and movement of particles. Optical tweezers have been used for cell sorting, actively alteration of polymer structures, application of stall forces, characterization of molecular motors and measurement of binding forces in the biological and medical fields.

For cellular manipulation and cell sorting techniques, optical tweezers have many advantages than other mechanical techniques. It is possible that *in vitro* manipulation of cells with light is sterile and without harming the cells. Trapping of up to 10 *Escherichia coli (E. Coli)* bacteria cells of 2 μm in length was trapped and manipulated by using 1064-nm laser tweezer quasi-simultaneously [24]. And control of the molecules in the cell without damaging cell wall is possible [25,26]. Altering the choromosome movement on to mitotic spindle *in vitro* [27], accelerating cell-cell interaction by bringing active retinal cells together [28], manipulation of vesicles for membrane fusion [29] can be examples of the studies for micromanipulation applications of optical tweezers.

Optical tweezers can be used to manipulate organelles. The trapping force on lipid granules inside yeast cell was measured between 10 and 60 pN due to change of viscosity of the yeast cells in 0.1-0.8 Pas range by 830-nm laser tweezer [30]. In

addition to inside cells, optical tweezers can be used in rheology and quantitative measurements of biological acitivites for *in vivo* applications. Flowing RBCs in blood capillaries of living animal was trapped and manipulated by infrared laser tweezers. The capillaries was blocked with RBCs and then was cleared with optical tweezers [31]. Also, cells and nanoparticles inside living zebrafish were trapped with 1064-nm laser [32].

In rheology applications, optical tweezers can be used for measurement the microscopic viscosity as a confocal probe [33] or they combined with optical microscopy in order to map the fluid flow and measure the viscosity [34,35]

Optical trapping in different surfaces has been developed in order to maximize efficiency of optical tweezers. Optical trapping of mammalian, yeast and *Escherichia coli* cells on the surface of two-dimensional photonic crystal was developed in order to minimize cell-damaging and increase cell viability in cell manipulation techniques [36]. The effect of trap position to focal waist in the vicinity of the reflecting surface in optical tweezer was studied [37]. As a surface, random gold nano-island substrates used for trapping of assembling of particles and live cells. Near-field optical trapping force and long-range thermophoretic force, which overcomes the axial convective drag force, creates trapping effect. Lateral convection pushes the samples into trapping region [38].

Two of the main applications of optical tweezers are study of molecular motors and physical properties of DNA. In both applications, biological sample is biochemically attached to polystyrene beads or glass beads in micron-sized range. By this way, the force and step size of the molecular motor can be measured. Block *et al.* improved the efficiency of kinesin motors as well as Svoboda *et al.* measured step size of kinesin on microtubules as 8 nm by combining with interferometry [39,40]. Moreover, elasticity of double and single stranded DNA molecules was determined by using optical tweezers [41]. Rigidity and bond breaking force was determined by applying torque to actin filaments [42]. In order to understand a cell division process of eukayotic organisms, minimum trapping force to move isolated single mammalian chromosome was determined to be ≈0.8-5 pN by using 1064 nm laser tweezer [43].

Mechanical properties of double-stranded DNA were determined by using 1064-nm laser tweezers [44].

Observing phase transitions in colloidal suspensions [45] and measuring entropic extraction in giant vesicles [46] can be set examples as applications of optical tweezers in colloidal systems.

For applications in statistical physics, escape of a Brownian particle from a coupled-tweezer trap was synchronized by using stochastic resonance [47]. Wang et al. experimentally demonstrated that the second law of thermodynamics has not been favorable for small systems and short timescales by using optical tweezers [48].

Besides polystene beads; absorbing particles [49], metallic particles [50,51,52], quantum dots [53], carbon nanotubes [54] and fluorescent beads[55] have also been trapped as well.

2. THE BASICS OF THE OPTICAL TWEEZER

2.1 Physical Principle of Optical Tweezer

Optical tweezers use the forces of laser radiation pressure to trap and manipulate microscopic particles. The trapping force (F_T) is a combination of two forces: a gradient force (F_G) and the scattering force (F_S) and determined by relation:

$$F_T = F_g + F_s \qquad (2.1)$$

The photon of the incident laser beam applies the pressure against the surface of the trapped particle and as result the gradient force arises whereas the scattering force arises from the change in velocity due to movement of light between mediums of two different indices of refraction. By the reason of the dependence of momentum on velocity and conservation of momentum, the trapped particle moves with equal but opposite momentum of the photons i.e. in the direction of incident light (Figure 2.1). [6].
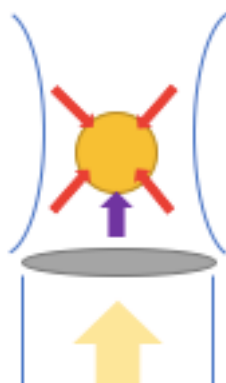
Figure 2.1: Optical forces. Gradient force is shown in red; scattering force is shown in purple.

If the size of the particles is larger than the wavelength of the trapping laser, principle of optical trapping is explained with ray optics; whereas particle is much smaller it is explained with dipole or Rayleigh approximation. In most experiments, the sizes of particles are comparable with the wavelength of the trapping laser. In this

case, instead of ray optics and Rayleigh approximation, electromagnetic theory of light is used. In order to calculate trapping forces in this range, generalized Lorenz-Mie theory is used [56,57].

2.1.1 Ray Optics approximation

The simple ray optics model of the single-beam gradient trap calculates the trapping forces on sphere of diameter larger than wavelength of light (R > 10 λ) [57,58].

In the ray optics or geometrical optics regime, total light beam is seperated into individual rays. Each ray has appropriate intensity, direction, polarization and the characteristics of a plane wave of zero wavelength. By this specs they can change directions by reflection and refraction and changes polarization according to the usual Fresnel formulas. This regime neglects diffractive effects [58].

Due to the neglect of surface reflection from the particle, the particle is trapped at the focus of the laser beam (Figure 2.2a). Therefore, there is no net force on the particle when the particle trapped at the focus. The particle leaving the traping the restoring force is formed to pull particle back to trap center (Figure 2.2b-c).

| (a) | (b) | (c) |
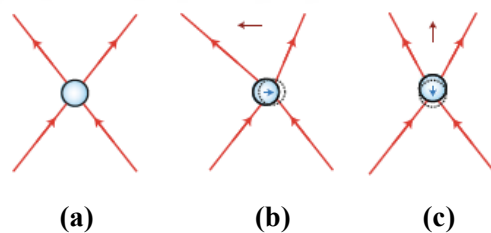
Figure 2.2: Qualitative view of optical trapping of dielectric spheres [57].

Whereas the surface reflection from the particle was neglected in above discussion; in reality, it has to be considered. Particle is pushed forward by the photons reflected back by the surface. In case of this force is greater than restoring force, particle is pushed forward and can not be trapped. The surface reflection depends on the relative refractive indices of the particle and the medium.

$$m = \frac{n_p}{n_{md}} \tag{2.2}$$

n_p and n_{md} are the refractive indexes of particle and medium, respectively. Larger m indicates more surface reflection and therefore greater difficulty in trapping the microsphere with an optical tweezer. In order to increase the restoring force, the laser

beam should be highly focused by a high numerical aperture (NA) objective lenses.

For the Ray optics approximation for single ray with power P, the gradient and scattering forces are determined as below (Figure 2.3).
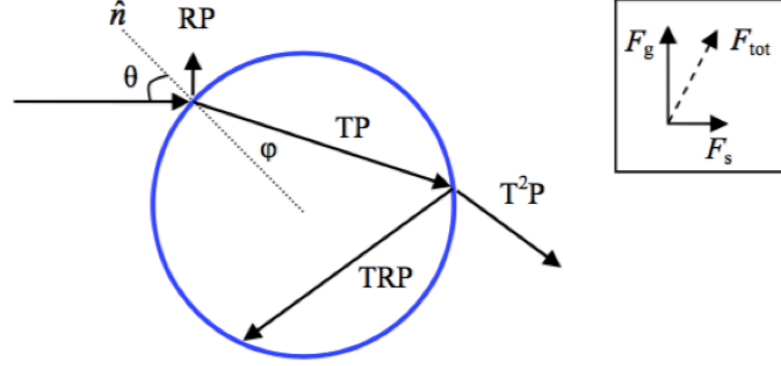
Figure 2.3: Ray propagation into dielectric sphere for ray optics approximation [25]. The ray is exposed both reflection, R and transmission T at all surfaces. $\hat{n}$ signifies the normal to the surface of the sphere.

$$F_S = \frac{n_{md}P}{c}\left(1 + R\cos 2\theta - T^2\frac{\cos(2\theta-2\varphi)+R\cos 2\theta}{1+R^2+2R\cos 2\varphi}\right) \tag{2.3}$$

$$F_g = \frac{n_{md}P}{c}\left(R\sin 2\theta - T^2\frac{\sin(2\theta-2\varphi)+R\sin 2\theta}{1+R^2+2R\sin 2\varphi}\right) \tag{2.4}$$

P is the power of the ray, θ and φ are the angles of the incident and refracted rays, respectively. $\frac{n_{md}P}{c}$ is the momentum per second transferred by the ray. R is Fresnel reflection coefficient and T is the fresnel transmission coefficient. These coefficients give the fraction of the light being reflected or transmitted at an interaction [25].

2.1.2 Rayleigh approximation

If the size of particle is smaller than the wavelength of the light (R < λ/10), the optical tweezer forces can be calculated by Rayleigh approximation [59]. The gradient in the electromagnetic field causes a force induced on the particle proportional to the gradient of the field and therefore proportional to the gradient of the intensity of the light. Intensity maximum is in the centre of the highly focused Gaussian beam for giving rise to a three-dimensional gradient of the laser light, which produces a force directed to the centre. The gradient force, F_g, is induced by

the field and described as,

$$F_g = \frac{2\pi a^3 n_{md}}{c} \left(\frac{m^2-1}{m^2+2}\right) \nabla I \tag{2.5}$$

c is the speed of the light, a is the radius of the object, m the effective index of reflection as described in equation (2.2) and I is the intensity of the light. It is shown that the gradient force is proportional to the volume of the particle and to the gradient of the intensity of the trapping light, i.e., $F_g \propto \nabla I$ [25,57].

The scattering force, F_s, is proportional to the intensity of the light and described as,

$$F_s = \frac{128\pi^5 a^6 n_{md}}{3\lambda^4 c} \left(\frac{m^2-1}{m^2+2}\right) I \tag{2.6}$$

The particle is attracted into the region of the highest intensity by gradient force, whereas the scattering force pulls the particle into an equilibrium position which is not at maximum intensity. Stable trapping is occured by competition of these forces [58,60]. Also, the size of the particle affects the gradient and scattering forces. For large particles, the scattering force is dominating and that it is resulted to trapping unstable [25].

2.1.3 Generalized Lorenz-Mie theory

When the sizes of particle are comparable with the wavelength of the trapping laser, electromagnetic theory of light has to be used [57,60]. Generalized Lorenz-Mie theory (GLMT) includes the equations of light scattering of a beam. Beam fields incident on the particle must be known for calculation of scattering by a transversely localized beam. The exact fields of beam complying with both the wave equation and Maxwell's equations are not in closed form, excepting plane wave. In order to explain this dificulty, transversely localized beam is expressed in 3 approaches: an angular spectrum of plane waves, the fields in terms of infinite series of spherical multipole partial waves with specified coefficients, analytic approximations of the beam field. GLMT calculations generally use second and third approaches [61].

For the fundamental TEM_{00} mode of laser beam, the electric and magnetic fields of a monochromatic Gaussiam beam is described as:

$$\boldsymbol{E}(x,y,z) = E_0 \exp\left(-\frac{\rho^2}{w_0^2}\right) \exp(ikz)\, \boldsymbol{u_x} \tag{2.7}$$

$$B(x, y, z) = (E_0/c) \exp\left(-\frac{\rho^2}{w_0^2}\right) \exp(ikz) \boldsymbol{u_y} \tag{2.8}$$

where c is the speed of the light, E_0 is the peak electric field strength, w_0 is the electric field half-width. The Gaussian beam of wavelength λ and wave number $k = 2\pi/\lambda$ is linearly polarized in the x direction and propagating in the +z direction. $\exp(i\omega t)$ is time dependence and it is implicit [61].

$$\rho^2 = x^2 + y^2 \tag{2.9}$$

If the center of the beam is at origin of coordinates, beam is on-axis related and thus it lies on the beam's symmetry axis.

Equations (2.7) and (2.8) ignore the diffraction of the beam. If the Gaussian beam fields are Fresnel diffracted from z=0 to z>0, electric and magnetic fields are defined as:

$$E(x, y, z) = DE_0 \exp\left(-\frac{D\rho^2}{w_0^2}\right) \exp(ikz) \boldsymbol{u_x} \tag{2.10}$$

$$B(x, y, z) = (DE_0/c) \exp\left(-\frac{D\rho^2}{w_0^2}\right) \exp(ikz) \boldsymbol{u_y} \tag{2.11}$$

where the D is given as:

$$D = \left(1 + \frac{2isz}{w_0}\right)^{-1} \tag{2.12}$$

where the s is beam confinement parameter and defined as:

$$s = 1/kw_0 \tag{2.13}$$

The beam becomes freely propagating focused Gaussian beam since it spreads tranversely with its minimum width w_0 in the z=0 plane. Beam confinement parameter has to be equal or less than $1/\pi$ because a beam must be tranversely confined at least of its wavelength. If the $s \ll 1/\pi$, a beam is loosely focused since its tranverse spreading goes on narrow and becomes only slowly as a function of z. If the $s \approx 1/\pi$, a beam is tightly focused since its tranverse spreading is wide and develops as a function of z. Equations (2.10) and (2.11) has the limits $w_0 \to \infty$ or $s \to 0$ which means that is a plane wave [61].

The diffracting Gaussian beam is favorable for the paraxial wave equation, but not

for full wave equation or Maxwell's equations. In order to obtain a beam in the form of infinite series in powers of s the procedure has been developed which is both exact solution of wave equation and Maxwell's equations. The procedure has the Gaussian beam of equations (2.10) and (2.11) as its zeroth order term [62,63]. s^5 order of the expansion of the beam fields is given as,

$$\boldsymbol{E}(x,y,z) = DE_0 \exp\left(-\frac{D\rho^2}{w_0^2}\right) \exp(ikz) \left[e_x\boldsymbol{u_x} + e_y\boldsymbol{u_y} - 2iD\left(\frac{x}{w_0}\right)e_z\boldsymbol{u_z}\right] \quad (2.14)$$

$$\boldsymbol{B}(x,y,z) = (DE_0/c) \exp\left(-\frac{D\rho^2}{w_0^2}\right) \exp(ikz) \left[b_x\boldsymbol{u_x} + b_y\boldsymbol{u_y} - 2iD\left(\frac{y}{w_0}\right)b_z\boldsymbol{u_z}\right] (2.15)$$

where

$$e_x = 1 + s^2\left(\frac{D}{w_0}\right)^2 \left[2x^2 + \rho^2 - D\left(\frac{\rho^4}{w_0^2}\right)\right]$$

$$+s^4\left(\frac{D}{w_0}\right)^4 \rho^2 \left[2\rho^2 + 8x^2 - 3D\left(\frac{\rho^4}{w_0^2}\right) - 2D\left(\frac{x^2\rho^2}{w_0^2}\right) + D^2\left(\frac{\rho^6}{2w_0^4}\right)\right] \quad (2.16)$$

$$b_y = 1 + s^2\left(\frac{D}{w_0}\right)^2 \left[2y^2 + \rho^2 - D\left(\frac{\rho^4}{w_0^2}\right)\right]$$

$$+s^4\left(\frac{D}{w_0}\right)^4 \rho^2 \left[2\rho^2 + 8y^2 - 3D\left(\frac{\rho^4}{w_0^2}\right) - 2D\left(\frac{y^2\rho^2}{w_0^2}\right) + D^2\left(\frac{\rho^6}{2w_0^4}\right)\right] \quad (2.17)$$

$$e_y = b_x = s^2\left(\frac{D}{w_0}\right)^2 (2xy) + s^4\left(\frac{D}{w_0}\right)^4 (2xy)\left[4\rho^2 - D\left(\frac{\rho^4}{w_0^2}\right)\right] \quad (2.18)$$

$$e_z = b_z = s + s^3\left(\frac{D}{w_0}\right)^2 \left[3\rho^2 - D\left(\frac{\rho^4}{w_0^2}\right)\right] +$$

$$s^5\left(\frac{D}{w_0}\right)^4 \rho^2 \left[10\rho^2 - 5D\left(\frac{\rho^4}{w_0^2}\right) + D^2\left(\frac{\rho^6}{2w_0^4}\right)\right] \quad (2.19)$$

In the above equations, s is determined as L approximation of the exact TEM$_{00}$ laser beam. s converges rapidly near the focal waist and slowly only when ρ^2 is greater than $w_0^2 + 4s^2z^2$. When the focal waist of the beam moved from the origin to other point which is favorable translation of coordinates, the translated beam is called off-axis related to scatterer whose center is not along the beam's symmetry axis [61].

It is assumed that exact electric and magnetic fields of the incident beam, which is considered as arbitrary tranversely localized, on a homogeneous sphere of radius a and refractive index n_p and centered at origin of coordinates, the TE and TM

12

Bromwich potentials of the beam in spherical coordinates are given by [61,64,65]

$$U_{TE}^{beam}(r,\theta,\varphi) = \sum_{n=1}^{\infty}\sum_{m=-n}^{n}\left(\frac{E_0}{k}\right) i^n c_n^{pw} g_{n,TE}^m \psi_n(kr) P_n^{|m|}[\cos(\theta)]\exp(im\varphi) \qquad (2.20)$$

$$U_{TM}^{beam}(r,\theta,\varphi) = \sum_{n=1}^{\infty}\sum_{m=-n}^{n}\left(\frac{E_0}{k}\right) i^n c_n^{pw} g_{n,TM}^m \psi_n(kr) P_n^{|m|}[\cos(\theta)]\exp(im\varphi) \qquad (2.21)$$

where

$$c_n^{pw} = (2n+1)/[2n(n+1)] \qquad (2.22)$$

E_0 is the maximum strength of the electric field of the beam. ψ_n and $P_n^{|m|}$ are the Ricatti-Bessel and Legendre functions, respectively. $g_{n,TE}^m$ and $g_{n,TM}^m$ are the beam shape coefficients. Electric and magnetic field are obtained by vector derivatives of equations (2.20) and (2.21). Beam shape coefficients is important for GLMT since the scattered intensity and all quantities derived from it are calculated by combination of beam shape coefficients, angular functions and a_n plane wave function of LMT and b_n partial wave function of LMT.

According to equations (2.20) and (2.21) and beam shape coefficients are given

$$g_{n,TE}^m = \left[\frac{(-i)^{n-1}}{2\pi}\right]\left[\frac{kr}{j_n(kr)}\right]\left[\frac{(n-|m|)!}{(n+|m|)!}\right]\int_0^\pi \sin(\theta)\,d\theta \int_0^{2\pi} d\varphi$$

$$\times P_n^{|m|}[\cos(\theta)]\exp(-im\varphi)\, cB_{rad}^{beam}(r,\theta,\varphi) \qquad (2.23)$$

$$g_{n,TM}^m = \left[\frac{(-i)^{n-1}}{2\pi}\right]\left[\frac{kr}{j_n(kr)}\right]\left[\frac{(n-|m|)!}{(n+|m|)!}\right]\int_0^\pi \sin(\theta)\,d\theta \int_0^{2\pi} d\varphi$$

$$\times P_n^{|m|}[\cos(\theta)]\exp(-im\varphi)\, E_{rad}^{beam}(r,\theta,\varphi) \qquad (2.24)$$

where E_{rad}^{beam} and B_{rad}^{beam} are the radial components of the presumably known beam fields in spherical coordinates. If the beam is on-axis in compliance with sphere, only m=±1 beam shape coefficients are not zero due to the structure of the φ integral and they are defined as:

$$g_{n,TE}^1 = -i g_{n,TE} \qquad (2.25)$$

$$g_{n,TE}^{-1} = i g_{n,TE} \qquad (2.26)$$

$$g_{n,TM}^{\pm 1} = g_{n,TM} \qquad (2.27)$$

If Gaussian beam propagates freely, $g_{n,TE}$ equals to $g_{n,TM}$. But more general beams

(laser beam) transmitted high numerical aperture lens $g_{n,TE}$ is different from $g_{n,TM}$. Since assuming that the Maxwell's equations are solved by the beam, the radial dependence of angular integrals stops the $kr/j_n(kr)$ which is prefactor. The resulting beam shape coefficients become constants. But if the beam shape coefficients are not solutions of Maxwell's equations, the beam shape coefficients are obtained from equations (2.23) and (2.24) without cancellations. In order to obtain constant coefficients, the value r is identified at a convenient location or right-hand side are integrated with respect to r from the origin to infinity. Both of these ways define a new beam by the beam shape coefficients by equations (2.20) and (2.21) in order to renormalize the original beam and repair the defect of not being exact solution of Maxwell's equation. The original beam is strongly resembled by the new beam in the region where the scattered fields are largest due to large field strength [61].

According to equations (2.20) and (2.21), for the scattering of beam by a sphere, scattered and interior Bromwich potentials are given,

$$U_{TE}^{scatt}(r,\theta,\varphi) = -\sum_{n=1}^{\infty}\sum_{m=-n}^{n}\left(\frac{E_0}{k}\right)i^n c_n^{pw} B_n^m \zeta_n^{(1)}(kr) P_n^{|m|}[\cos(\theta)]\exp(im\varphi) \quad (2.28)$$

$$U_{TM}^{scatt}(r,\theta,\varphi) = -\sum_{n=1}^{\infty}\sum_{m=-n}^{n}\left(\frac{E_0}{k}\right)i^n c_n^{pw} A_n^m \zeta_n^{(1)}(kr) P_n^{|m|}[\cos(\theta)]\exp(im\varphi) \quad (2.29)$$

and

$$U_{TE}^{interior}(r,\theta,\varphi) = \sum_{n=1}^{\infty}\sum_{m=-n}^{n}\left(\frac{NE_0}{k}\right)i^n c_n^{pw} D_n^m \psi_n(Nkr) P_n^{|m|}[\cos(\theta)]\exp(im\varphi) \quad (2.30)$$

$$U_{TM}^{interior}(r,\theta,\varphi) = \sum_{n=1}^{\infty}\sum_{m=-n}^{n}\left(\frac{NE_0}{k}\right)i^n c_n^{pw} C_n^m \psi_n(Nkr) P_n^{|m|}[\cos(\theta)]\exp(im\varphi) \quad (2.31)$$

where $\zeta_n^{(1)}$ are Ricatti-Henkel functions, A_n^m and B_n^m are defined as partial wave scattering amplitudes and C_n^m and D_n^m are described as the partial wave interior amplitudes. These are obtained by matching the boundary conditions for various components of electric and magnetic fields at the sphere:

$$A_n^m = a_n g_{n,TM}^m \tag{2.32}$$

$$B_n^m = b_n g_{n,TE}^m \tag{2.33}$$

$$C_n^m = c_n g_{n,TM}^m \tag{2.34}$$

$$D_n^m = d_n g_{n,TE}^m \tag{2.35}$$

The scattered fields are various vector derivatives of the Bromwich potentials of equations (2.30) and (2.31). For the r goes to infinity, scattered intensity defined as

$$I_{scatt}(r,\theta,\varphi) = (E_0^2/\mu_0 c)(1/kr)^2[|S_1(\theta,\varphi)|^2 + |S_2(\theta,\varphi)|^2] \qquad (2.36)$$

where μ_0 is permeability of free space and the $S_1(\theta,\varphi)$ and $S_2(\theta,\varphi)$ are the total scattering amplitudes.

$$S_1(\theta,\varphi) = -\sum_{n=1}^{\infty}\sum_{m=-n}^{n} c_n^{pw}[-im\, a_n g_{n,TM}^m \pi_n^{|m|}(\theta) + b_n g_{n,TE}^m \tau_n^{|m|}(\theta)]\exp(im\varphi) \quad (2.37)$$

$$S_2(\theta,\varphi) = -\sum_{n=1}^{\infty}\sum_{m=-n}^{n} c_n^{pw}[-im\, b_n g_{n,TE}^m \pi_n^{|m|}(\theta) + a_n g_{n,TM}^m \tau_n^{|m|}(\theta)]\exp(im\varphi) \quad (2.38)$$

and the angular functions are defined as below.

$$\pi_n^{|m|}(\theta) = \left[\frac{1}{\sin(\theta)}\right]P_n^{|m|}[\cos(\theta)] \qquad (2.39)$$

$$\tau_n^{|m|}(\theta) = (d/d\theta)P_n^{|m|}[\cos(\theta)] \qquad (2.40)$$

GLMT formulas have also been derivations of the scattered power and scattered cross section [64], the radiation force on the sphere [64,66,67] and the radiation torque [66,68].

This method becomes complex when hundreds and thousands are required for scattering of beam from large particle with $2\pi a/\lambda \gg 1$. If the s≪1, localized model of the coefficients which is based upon van de Hulst's association in LMT of the incident ray impact parameter kρ with partial wave number n+1/2 is an alternative to this method. Given the fact that the center of a Gaussian beam's focal waist is located at $(x_0 = \rho_0\cos(\varphi_0), y_0 = \rho_0\sin(\varphi_0), z_0)$, the localized model coefficients are defined below [69,70].

$$g_{n,TE}^m = (-iF_n)[-iexp(-i\varphi_0)/(n+1/2)]^{m-1}[I_{m-1}(Q) - \exp(-2i\varphi_0)I_{m+1}(Q)] \quad (2.41)$$

$$g_{n,TE}^0 = F_n\left[\frac{2in(n+1)}{(n+1/2)}\right]\sin(\varphi_0)I_1(Q) \qquad (2.42)$$

$$g_{n,TE}^{-m} = (-iF_n)[-iexp(i\varphi_0)/(n+1/2)]^{m-1}[I_{m-1}(Q) - \exp(2i\varphi_0)I_{m+1}(Q)] \quad (2.43)$$

$$g_{n,TM}^m = F_n[-iexp(-i\varphi_0)/(n+1/2)]^{m-1}[I_{m-1}(Q) - \exp(-2i\varphi_0)I_{m+1}(Q)] \qquad (2.44)$$

$$g_{n,TM}^0 = F_n\left[\frac{2in(n+1)}{(n+1/2)}\right]\cos(\varphi_0)I_1(Q) \qquad (2.45)$$

$$g_{n,TM}^{-m} = F_n[-iexp(i\varphi_0)/(n+1/2)]^{m-1}[I_{m-1}(Q) - \exp(2i\varphi_0)I_{m+1}(Q)] \qquad (2.46)$$

where

$$F_n = D_0 \exp\left(-\frac{D_0\rho_0^2}{w_0^2}\right) exp\left[-D_0 s^2\big((n+1/2)\big)^2\right]\exp\left(-ikz_0\right) \qquad (2.47)$$

$$D_0 = \left[1 - 2is\left(\frac{z_0}{w_0}\right)\right]^{-1} \qquad (2.48)$$

$$Q = 2D_0 s(n+1/2)(\rho_0/w_0) \qquad (2.49)$$

and I_m are modified Bessel functions.

When the beam is on-axis, these focused Gaussian beam coefficients as simplified as

$$g_{n,TE} = g_{n,TM} = D_0 exp[-D_0 s^2(n+1/2)^2]\exp\left(-ikz_0\right) \qquad (2.50)$$

In the plane wave, $g_{n,TE} = g_{n,TM} = 1$ limits the LMT. The localized beam shape coefficients in equations (2.20) and (2.21) define a beam which is exact solution of Maxwell's equations. It has been studied the reason why localized beam shape coefficients are related to Fresnel diffracted fields rather than Davis-Barton fields [71,72,73,74,75]. The localized model coefficients are derivation of general principles, and the beam defined by the localized coefficients performs to expect the behavior of the higher order Davis-Barton beams.

For other beam types, localized models have been derived from GLMT scattering calculations for scattering of a beam with s≪1 and large particle with $2\pi a/\lambda \gg 1$ [75,76,77,78,79,80]. Localized models have been developed for scattering by a circular [81] or elliptical cylinder [82]. Also, the procedure used experimently in order to measure beam shape coefficients [83,84].

By the means of beam shape coefficients, optical force can be calculated by using cross sections in x, y and z axis for radiation force [59,64].

$$\boldsymbol{F(r)} = \frac{n_{md}}{c}I_0\left[\hat{\boldsymbol{x}}C_{pr,x}(\boldsymbol{r}) + \hat{\boldsymbol{y}}C_{pr,y}(\boldsymbol{r}) + \hat{\boldsymbol{z}}C_{pr,z}(\boldsymbol{r})\right] \qquad (2.51)$$

where P is the power of the laser and I_0 equals to intensity of beam at center of the beam and determined as $I_0=2P/\pi w_0^2$ [59]. $C_{pr,i}$ are cross-sections [59,64,85,86].

2.2   Trapping Efficiency

For optimizing the optical trapping, trapping efficiency must be considered as well as magnitude of the trapping force on the dielectric particle. The force is related to trapping beam power.

$$F = \frac{Qn_{md}P}{c} \qquad (2.52)$$

where F is force on the particle in an optical trap, Q is defined trapping efficiency, P is the beam power of the laser at trapping plane. Higher Q means higher trapping efficiency. $n_{md}P/c$ defines the incident flux from the laser in a medium with refraction index n_{md}, c is the speed of the light trapping [87].

Intensity distribution of the light at entrance of the microscope determines the trapping efficiency. In Ray optics approximation, it is predicted that overfilling the microscope objective can make the efficiency higher. Diameter of the incident laser beam is greater then the objective opening, trimming the outer portion of the beam. The farther rays entering the objective with steepest angles, make an increase in intensity related to central on-axis beams. Thus, the axial trapping efficiency increases since gradient force is getting greater than scattering force. For lateral trapping, the effect of overfilling is clear since particle size have come up with conflict results.

2.3   Detection and Calibration of Optical Forces

2.3.1   Force detection techniques

Optical tweezers can measure and apply forces on spheres besides trapping the particles for manipulation. The particle is confined in a three-dimensional harmonic potential by optical trap (Figure 2.4). Single direction of this potential can be defined as $E(x)=kx^2/2$ where k is a harmonic constant. The force is linearly dependent on the displacement. In order to determine the force, position of the bead in a trap should be measured [25].
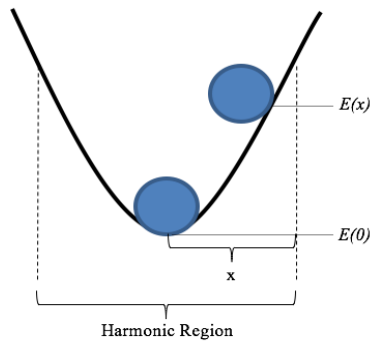
Figure 2.4 : Trapped particle confined in harmonic potential.

In order to measure the position of the trapped particle, quadrant photodiode (QPD) or standard video camera with subsequent particle tracking can be used. QPD measures smaller forces with high time resolutions and nanometer sized displacements at a rate of several kHz. They offer precise, high-bandwidth measurements. However, tracking multiple particles with QPD simultaneously is difficult. Although standard video cameras allow tracking multiple particles with an accuracy of the order of 10 nm and frame rate of about 30 Hz, this frame rate is often slower than typical resonance frequency of an optical trap. High-speed video camera is an alternative to QPD and standard video camera for recording positions of many particles at several kHz. It is showed that both high-speed, full-field , CCD camera and QPD have similar performance for measuring displacement in optical tweezers [88]. CMOS cameras provide reduced field of view frame rates of the order 1kHz, and the data can be managed in real time using a stardard PC [89,90].

2.3.2   Calibration techniques

Various methods for measuring trap forces have been studied. Firstly, there is a drag force method which allows to calculate stiffness and trapping force by using velocity and viscosity of fluid. Second method is equipartition method or Brownian Motion method. In this method, trap force is measured by Boltzmann's constant, absolute temperature and position data of particle. Escape force methods calculates the force by escape velocity which can be measured by accelerating the particle until it gets out from the optical trap. Fourth method is the power spectrum method which uses the thermal vibrations for calculating stiffness. Last method is step response method which is based on estimation of trapped bead's response according to movement of the trapped focus [7,8].

2.3.2.1 Drag force method

The viscosity and velocity of fluid, size and shape of particles must be known for this method. In this method sample is moved at constant velocity, the occurring force causes displacement of the bead from the laser, x [8]. Stiffness, k, can be calculated as given,

$$k = F_{trap}/x \qquad (2.53)$$

where F_{trap} is trapping force. Trapping force equals to the drag force since drag force can not break the trapping action.

$$F_{trap} = F_{drag} = 6\pi\mu v_f a \qquad (2.54)$$

where the μ is the dynamic viscosity of the fluid, v_f is the velocity of the fluid and a is the radius of the particle.

2.3.2.2 Brownian Motion method

Particles suspended in fluid moves randomly due to the collisions with the moving molecules of liquid. This is called as The Brownian Motion. The Brownian motion method uses the thermal fluctuation of the trapped particle, using absolute temperature to measure trap stiffness, k. This stiffness of the tweezer is calculated from the equipartition theorem for a particle fluctuating in a harmonic potential of the trap [7,8]. In equipartition theorem, a molecule in thermal equilibrium has a kinetic energy for each degree of freedom $<H>$. Assuming that the movement of the trapped particle is resulted from only thermal fluctuations, kinetic energy equals to potential energy of the trap:

$$\langle H \rangle = \frac{1}{2} k_b T = \frac{1}{2} k \langle x^2 \rangle \qquad (2.55)$$

where the k_b is the Boltzmann's constant, k_b=1.3807x10^{-23} JK^{-1} and the T is the absolute temperature. $<x^2>$ is the time-averaged square of the bead's horizontal displacement from the center of the trap. In this method, either particle geometry or viscosity of fluid is not required to calculate the stiffness. The temperature causes random vibration and trap force resists movement from the trap center [7].

2.3.2.3 Escape force method

It was the first method to estimate optical trapping [2]. In this method, the force required on the particle to escape from the trap. If the particle slowly is accelerated until it breaks from its trap, the escape force can be measured (Figure 2.5). The trap force simply equals to the escape force caused by the acceleration [8].

$$F_{trap} = F_{escape} = 6\pi\gamma v_c a \qquad (2.56)$$

γ is a drag coefficient, a is the radius of the particle and v_c is the escape velocity.
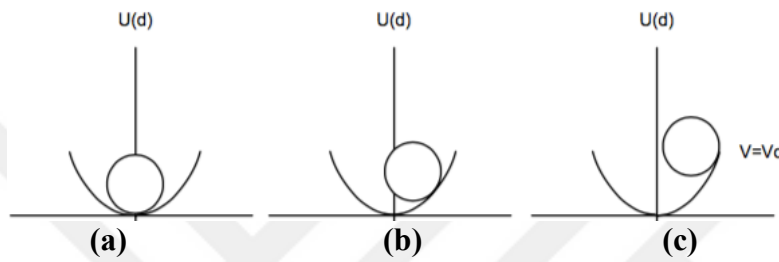
Figure 2.5: Potential energy of the beads displaced by the optical tweezer at different velocities [8].

At first the particle is trapped on the bottom of the potential well of the optical trap. And then, drag force is active and it produces displacements, the bead is placed at the edge of the trap v_c.

2.3.2.4 Power spectrum method

In this method, the stiffness is calculated by determining the power spectrum of the movement of trapped particle [8]. In the harmonic potential of the trap, the particle motion can be explained with Langevin equation and given

$$F(t) = \gamma\dot{x} + kx \qquad (2.57)$$

where, x is the deviation from the equilibrium, k is the trap spring constant, γ is a drag coefficient and *F(t)* is the fluctuation force due to random vibration of the molecules in the fluid. In order to find out fluctuating *x(t)*, position of the bead is recorded with respect to time. And then, the power spectrum for *x(t)* is found by taking the Fourier transform and the modulus squared to obtain

$$S(f) = \frac{k_b T}{\beta\pi^2(f^2+f_c^2)} \qquad (2.58)$$

where f_c is corner frequency [91,92], $f_c = k_x/2\pi\beta$ and $\beta = 6\pi\gamma a$.

2.3.2.5 Step response method

In this method, the response data of the particle's movement is taken by moving the trap focus stepwise [93]. The particle displaced by small offset and the subsequent trajectory of trapped bead is recorded. By rapid displacement, the large external force occurs on bead which is called as restoring force. The stiffness calculated by,

$$k = \frac{\beta}{\tau} \tag{2.59}$$

where, τ is the time constant [94]. When the particle trapped at the center of the focus, particle does not suffer restoring force towards the trap center.
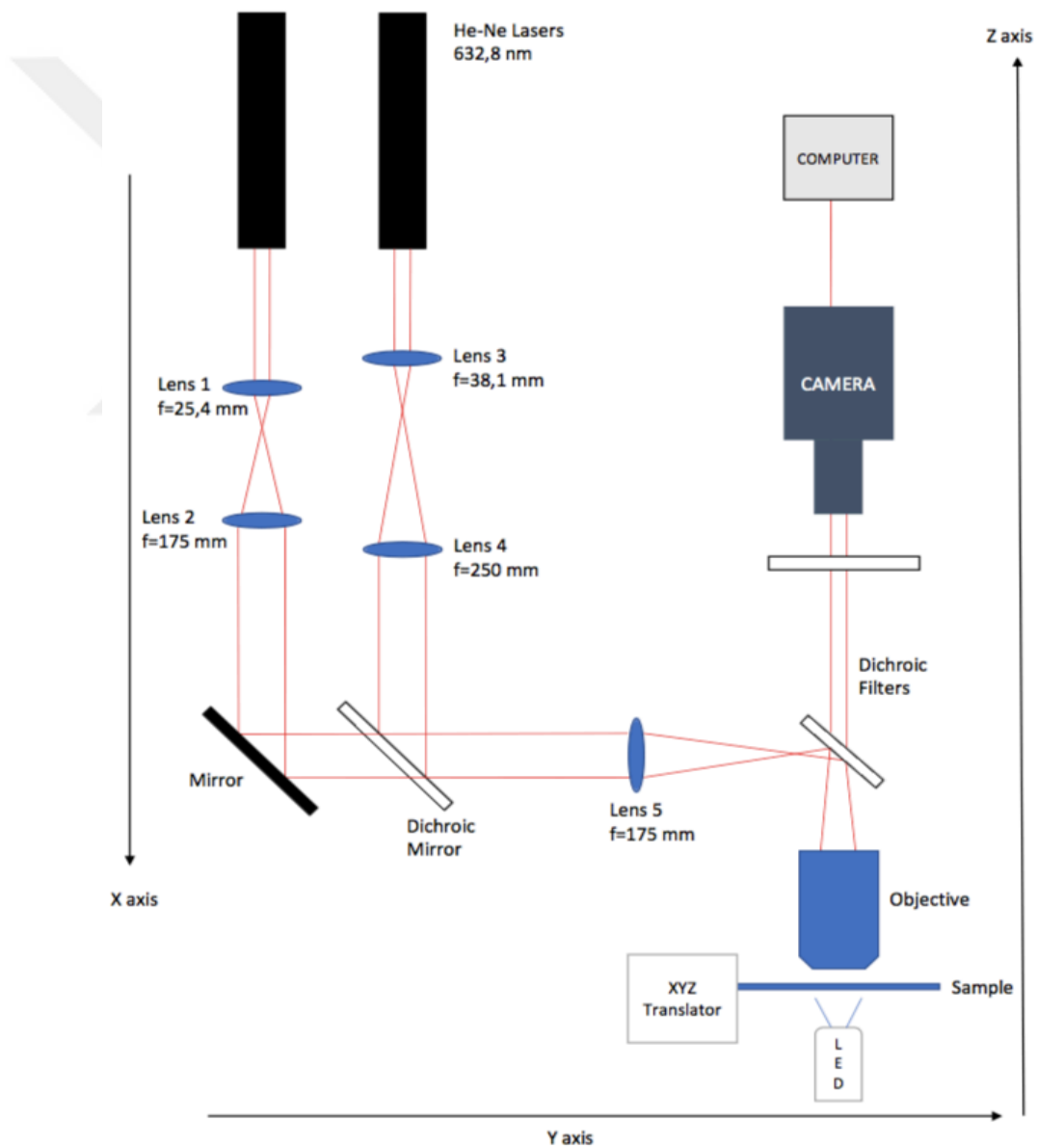
3. THE BASIC ELEMENTS OF OPTICAL TWEEZER

In this section, components of optical tweezer are described. This optical tweezer consists of two focused laser beams to trap the objects, a sample manipulating system, and an imaging system used to monitor the experiment (Figure 3.1).

Figure 3.1: The setup of the optical tweezer.

3.1 Trapping Optics

Maximizing the trap depth means maximizing gradient intensity (∇I) at the trapping focus. When the microscope objective and lasers are chosen, trap depth can be maximized by adjusting the beam size and radius of curvature of the light incident on the microscope objective [95].

Increase in ∇I causes reduction in trap depth as long as the total power is held constant. The trap depth (ω_{trap}) is limited by the diffraction of the light but it can be overcomed with particular laser and microscope objective. ω_{trap} is obtained by an lens of focal length f focusing on a collimated laser beam with a diameter D:

$$\omega_{trap} \geq \frac{1.22\,f\lambda}{2D} = \frac{1.2\lambda_0 \tan\left[\sin^{-1}\left(\frac{NA}{n_{md}}\right)\right]}{n_{md}} = \frac{1.22\lambda_0}{n_{md}}\sqrt{\left(\frac{n_{md}}{NA}\right)^2 - 1} \qquad (3.1)$$

where NA is the numerical aperture of the lens, and n_{md} is the refractive index of the medium, λ_0 is the wavelength of the laser.

Equalization of diameter of the incident light at the objective, d_{obj}, and the diameter of the objective, D_{obj}, makes the trap strongest. If d_{obj} is less than D_{obj}, ω_{trap} will be greater than the minimum value for the lens, and it causes a reduction in strength of the trap. If d_{obj} is greater than D_{obj}, all of the light can not be transmitted through the objective. Therefore, ω_{trap} has the minimal value whereas the intensity and the intensity gradient is lower. Since the diameter of the output of lasers are smaller than D_{obj}, in order to transform the output of the laser into a collimated beam and make the diameter equals to objective, telescopes are formed. [95].

3.1.1 Lasers

The output beam shape, the beam astigmatism, the power and the wavelength are the four important characteristics of lasers. The output beam shape and the beam astigmatism effects focusing of the laser by the objective. Laser should have a single tranverse mode output with good beam quality for focusing to a single spot.

The laser wavelength is preferred by the applications of the trap. For manipulating objects such as polystyrene beads, visible lasers are appropriate. For biological specimens, absorption of visible lasers can damage the specimen whereas the

absorption of infrared lasers are less and therefore light sources with wavelengths range from 750 nm to 1000 nm can be used. The HeNe lasers which have 632.8 nm wavevlength are used in this custom designed optical tweezer system.

3.1.2 Lenses

In order to create collimated beam with a diameter equal to diameter of the microscope objective, telescope is used. Simple telescope has two convex lenses, L_1 and L_2, with focal lengths f_1 and f_2, respectively and the distance between them is $d_1 = f_1 + f_2$, and the magnification, M equals to $\frac{L_2}{L_1}$. The telescope, T_1, which is used for first laser is composed of two biconvex lenses, L_1 and L_2, with focal lengths 25,4 and 175 mm, respectively. And the telescope, T_2, which is used for second laser is composed of two biconvex lenses, L_3 and L_4, with focal lengths 38.1 and 250 mm, respectively.

3.1.3 Sending the light through the objective

The light is sent into the objective after telescope by mirrors and lens with focal length 175 mm. The collimated beam which exits first telescope, T_1, goes through the mirror and reflects to the lens, L_5, which makes the beam diameter equals to diameter of the objective. The laser beam goes to the dichroic mirror, which allows to first laser beam get through it, and is reflected to the curvature lens, L_5. After L_5, the laser beams are reflected by the dichroic mirror in adjustable mount to center and make the light perpendicular on the objective.

3.1.4 Objective

Objective (RMS100X-O, 100X Olympus Plan Achromat Oil Immersion Objective, 1.25 NA, 0.150 mm WD) that requires the usage of oil between microscope objective and cover slip is used. Trapping is possible but more difficult with lower magnification or lower numerical aperture objectives, so they are not recommended.

3.2 Sample manipulation

In order to trap objects in aqueous medium, standard microscope slide and cover slip is used. Translator is used to move the sample in micro-sized range. Also, changing

alignment of the laser into objective provides very fine changes in the position of the trapped particles.

3.3 Imaging System

The trapping objective is used for the imaging system. The imaging light is chosen as LED. The reason why the both trapping light and the imaging light pass through the same objective, CCD camera (DCU223M   CCD Camera, 1024 x 768 Resolution, B&W) was used for the imaging trapped particle. As a dichroic beam splitter, dichroic green filter is chosen since it permits transmittance of the imaging light and reflection the trapping light. Two beams follow the way between objective and CCD but only the imaging light reach the viewers to image trapped particle.

4.   THE ALIGNMENT PROCEDURE

The setup of the optical tweezer begins with the alignment of the laser beam. At first the beams are aligned with diaphragm which are attached to posts and rail carriers. After that, the mirrors are placed in kinematic mirror mounts which allow the mirrors' vertical and horizontal angle to be changed. Lenses used in optical tweezer are mounted on the rails assembly using posts and rail carriers. The lens height must be adjusted so that the laser beams pass through them. Once alignment complete, the diaphragms are removed from the rail. The maximum trapping force can be achieved when the diamater of the beam entering the objective equals the diameter of the objective. Lens 1 and lens 2 form telescope 1, lens 3 and lens 4 form telescope 2. All lenses of telescopes are bi-convex. Telescopes are used to expand the beams to correct diamaters and collimate them. In order to minimize the divergence of the inicdent beam, the telescopes should be placed as close as the lasers.

The light is sent into the objective after telescope by mirrors and lens 5 with focal length 175 mm which is plano-convex. The collimated beam which exits first telescope, T_1, goes through the mirror and reflects to the lens, L_5, which makes the beam diameter equals to diameter of the objective. The second laser beam which exits the telescope 2, T_2, goes to the dichroic mirror, which allows to first laser beam get through it, and is reflected to the curvature lens, L_5. The way of the light between the output of the laser and objective is set up by using mirrors. Mirrors are held in adjustable mounts, which can control the angle between mirror and two orthogonal axes, and reflect the light. Angles and positions of lasers are controlled by these mirrors independently. After L_5, the laser beams are reflected by the dichroic mirror in adjustable mount to center and make the light perpendicular on the objective. 100× objective with numerical aperture 1.25 that requires the usage of oil between microscope objective and cover slip is used.

The correct distances between optical components can be calculated by using Gaussian Beam Optics.

4.1 Gaussian Beam Optics

Focusing, modifying or shaping the laser beam by lenses or other optical equipments is required for most laser applications. In general, it is assumed that laser beam propagates approximately Gaussian beam, and it has Gaussian beam intensity profile which corresponds to theoretical TEM_{00} mode. In TEM_{00} mode, the laser beam begins as a perfect plane wave with a Gaussian transverse intensity (Figure 4.1). The output of real-life lasers is not truly Gaussian while He-Ne and argon-ion lasers are very close approximation [96].
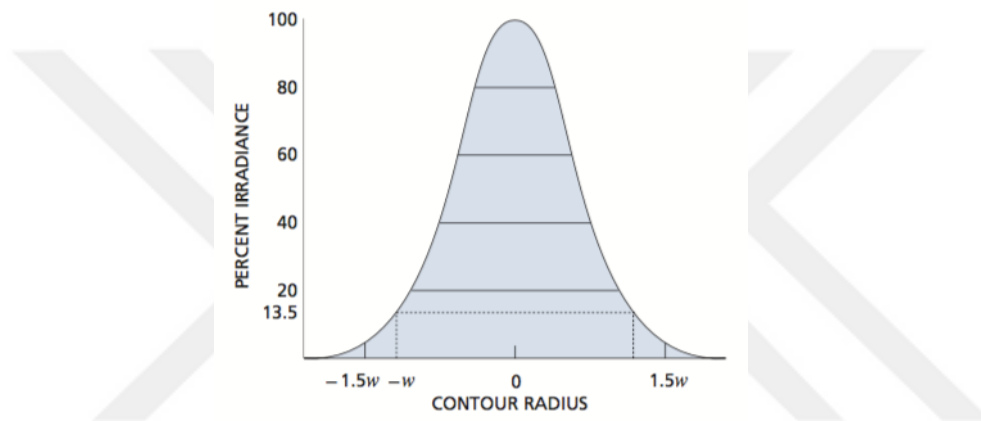
Figure 4.1: Irradiance profile of a Gaussian TEM_{00} mode [96]**.**

The Gaussian beam is trimmed at some diameter by some limiting optical aperture or internal dimensions of the laser in order to determine the propagation characteristics of a laser beam. There are two definitions about it. First one is the diameter at which the beam irradiance has decreased to $1/e^2$ of its peak or axial value. Second one is referred to as FWHM, full width at half maximum, since diameter at which the beam radiance has decreased to 50% of its peak or axial value (Figure 4.2) [96].
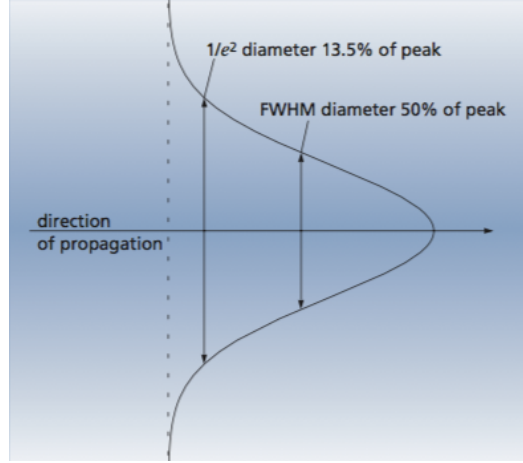
Figure 4.2: Diameter of a Gaussian beam [96].

For the lasers which are operating in TEM$_{00}$ mode, the irradiance is given by Gaussian function:

$$I(r) = I_0 e^{-2r^2/w^2} = \frac{2P}{\pi w^2} e^{-2r^2/w^2} \tag{4.1}$$

where w is the distance out from the center axis of the beam where the irradiance falls to $1/e^2$ of its value on axis. P is total power of the beam and r is defined as the transverse distance from the central axis. w depends on the distance z that the beam has propagated. w_0 is the radius of the $1/e^2$ irradiance [96].

The beam size will increase, slowly at first, then faster, eventually increasing proportional to z. The curvature of wavefront which was infinite at z=0, will become finite and initially decrease with z. When it reaches the minimum value, then increase with larger z, eventually proportional to z [96,97].

$$R(z) = z\left[1 + \left(\frac{\pi w_0^2}{\lambda z}\right)^2\right] \tag{4.2}$$

$$w(z) = w_0 \left[1 + \left(\frac{\lambda z}{\pi w_0^2}\right)^2\right]^{1/2} \tag{4.3}$$

$w(z)$ is the radius of the $1/e^2$ contour after the wave has propagated a distance z, and $R(z)$ is the wavefront radius of curvature after propagating a distance z.

The total beam behavior is defined by two parameters above since they occur in the same combination in both equations, they are often combined into a single parameter, z$_R$, the Rayleigh range:

$$z_R = \frac{\pi w_0^2}{\lambda} \tag{4.4}$$

R has its minimum value at z= z_R. Rayleigh range is the distance from the beam waist to the point at which beam radius has increased to $\sqrt{2}\, w_0$ [97] .

In the condition of z>>z_R, the beam starts to diverge as a spherical wave. The diverging beam has a full angular width θ:

$$\theta = \frac{4\lambda}{2\pi w_0} \tag{4.5}$$

When the origin gets closer to a point source and tanθ≈θ, θ is given by geometrical optics by division of the diameter of illumination on the lens, d, to the focal length of the lens, f (Figure 4.3).
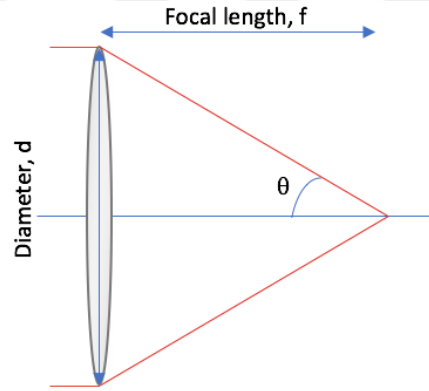
Figure 4.3: Tangent approximation.

$$\theta \approx \frac{d}{f} = \left(f/_\# \right)^{-1} \tag{4.6}$$

where f/# is defined as the photographic f-number of the lens. Beam waist diameter can be found as given

$$2w_0 = \left(\frac{4\lambda}{\pi} \right) \left(\frac{f}{d} \right) \tag{4.7}$$

And also depth of focus (DOF) shown in figure 4.4 can be defined as the distance between the values of z at $w = \sqrt{2}w_0$ given as below[98].

$$DOF = \left(\frac{8\lambda}{\pi} \right) \left(\frac{f}{d} \right)^2 \tag{4.8}$$

4.1.1 Gaussian beam propagation and ABCD matrices

If the Gaussian beam propagates in free space, the spot size of the beam and radius of curvature at z are given above. The real and imaginary parts of both spot size and radius of curvature is contained by the complex radius of curvature *q(z)* [99, Page 81]. Since *q(z)* varies according to

$$q(z) = z + iz_R \tag{4.9}$$

The inverse of *q(z)* contains lots of information about Gaussian beam and it is given as below.

$$\frac{1}{q(z)} = \frac{1}{z+iz_R} = \frac{z}{z^2+z_R^2} - i\frac{z}{z^2+z_R^2} \tag{4.10}$$

Equation (4.10) can be written by using w_0, *w(z)* and *R(z)*.

$$\frac{1}{q(z)} = \frac{1}{R(z)} - \frac{i\lambda_0}{\pi n w^2(z)} \tag{4.11}$$

If the initial value of *q(0)* is determined by using equations (4.10) and (4.11), *R(z)* and *w(z)* can be calculated for different z values as the beam propagates. It means that calculation of *q(z)* is simplified and it is able to be known the behaviour of the Gaussian beam about calculation of the paraxial wave equation [99]. *q(z)* can be calculated by using ABCD matrices. The ABCD matrix is a characteristic of each optical element.

r and θ coordinates of before and after an optical element have a linear relation (Figure 4.4).
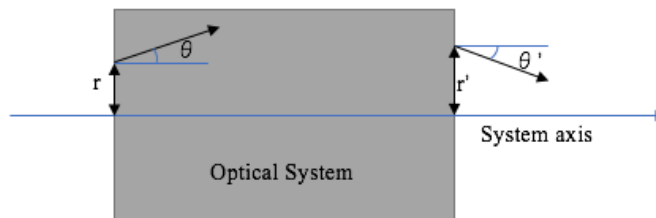
Figure 4.4: r and θ coordinates of optical system.

$$\begin{bmatrix} r' \\ \theta' \end{bmatrix} = \begin{bmatrix} A & B \\ C & D \end{bmatrix} \begin{bmatrix} r \\ \theta \end{bmatrix} \tag{4.12}$$

$$r' = Ar + B\theta \tag{4.13}$$

$$\theta' = Cr + D\theta \tag{4.14}$$

r and r' are the positions of the input and output of an optical element, respectively. θ is an angle at the input and θ' is an angle at the output with respect to the optical axis [100].

If q_1 and q_2 are signified as parameters of Gaussian beam at the input and output of the optical element, respectively, the optical element can be described by using ABCD matrix as below [99].

$$q_2 = \frac{Aq_1 + B}{Cq_1 + D} \tag{4.15}$$

At distance d in free space, since wave propagates along beams, coordinates of the beam change according to equations $r' = r + \theta d$ and $\theta' = \theta$ [100]. The transmission matrix M is therefore

$$M = \begin{bmatrix} 1 & d \\ 0 & 1 \end{bmatrix} \tag{4.16}$$

For refraction on planar boundary which created by two medium of refraction indexes n_1 and n_2, angles of the beam change according to Snell's law [100].

$$n_1 \sin(\theta) = n_2 \sin(\theta') \tag{4.17}$$

In paraxial approximation, $n_1\theta \approx n_2\theta'$ and therefore, position of the beam stays unchanged $r'=r$. The transmission matrix is written as

$$M = \begin{bmatrix} 1 & 0 \\ 0 & n_1/n_2 \end{bmatrix} \tag{4.18}$$

For a Gaussian beam which propagates through thin lens of the focal length f, distance from the axis is unchanged and axial equation can be written as

$$\theta' = \theta - \frac{r}{f} \tag{4.19}$$

f is greater than 0 for convex lenses and f is less than 0 for concave lenses. The transmission matrix is written for thin lenses as below [100].

$$M = \begin{bmatrix} 1 & 0 \\ -1/f & 1 \end{bmatrix} \tag{4.20}$$

For reflecting beam from planar mirror, angles and positions do not change ($r=r'$ and $\theta = \theta$'). The transmission matrix is unitary.

$$M = \begin{bmatrix} 1 & 0 \\ 0 & 1 \end{bmatrix} \tag{4.21}$$

However for spherical mirror which has radius R, output values differ from input values [100].

$$\theta' + \theta = \frac{2r}{-R} \tag{4.22}$$

And the transmission matrix for reflection from spherical mirror can be written as

$$M = \begin{bmatrix} 1 & 0 \\ 2/R & 1 \end{bmatrix} \tag{4.23}$$

R is less than 0 for convex mirror and f is greater than 0 for concave mirror [99].

If the tranmisson matrices of optical components order from the output of the laser as M_1, M_2, M_3..M_z to distance z, transmission matrix of the complete optical system is calculated as

$$M = M_z \ldots M_3 M_2 M_1 \tag{4.24}$$

In order to find a beam waist by using ABCD matrices, the initial position of the beam waist must be located at z=0 with the radius of Gaussian distribution (w_0) [101].

$$BD + ACq^2 = 0 \tag{4.25}$$

$$w_1^2 = \frac{w_0^2}{(AD-BC)}\left(A^2 + \frac{B^2}{q^2}\right) \tag{4.26}$$

New position and radius of the beam waist for a condition of refractive index=1 can be solved with equation (4.25) and (4.26), respectively.

$$q = \frac{\pi w_0^2}{\lambda} \tag{4.27}$$

5. LASER SETUP

The distances between optical components are defined experimentally and theoreatically by using MATLAB (Figure 5.1 and Table 5.1). Power was measured after optical components (Table 5.2).
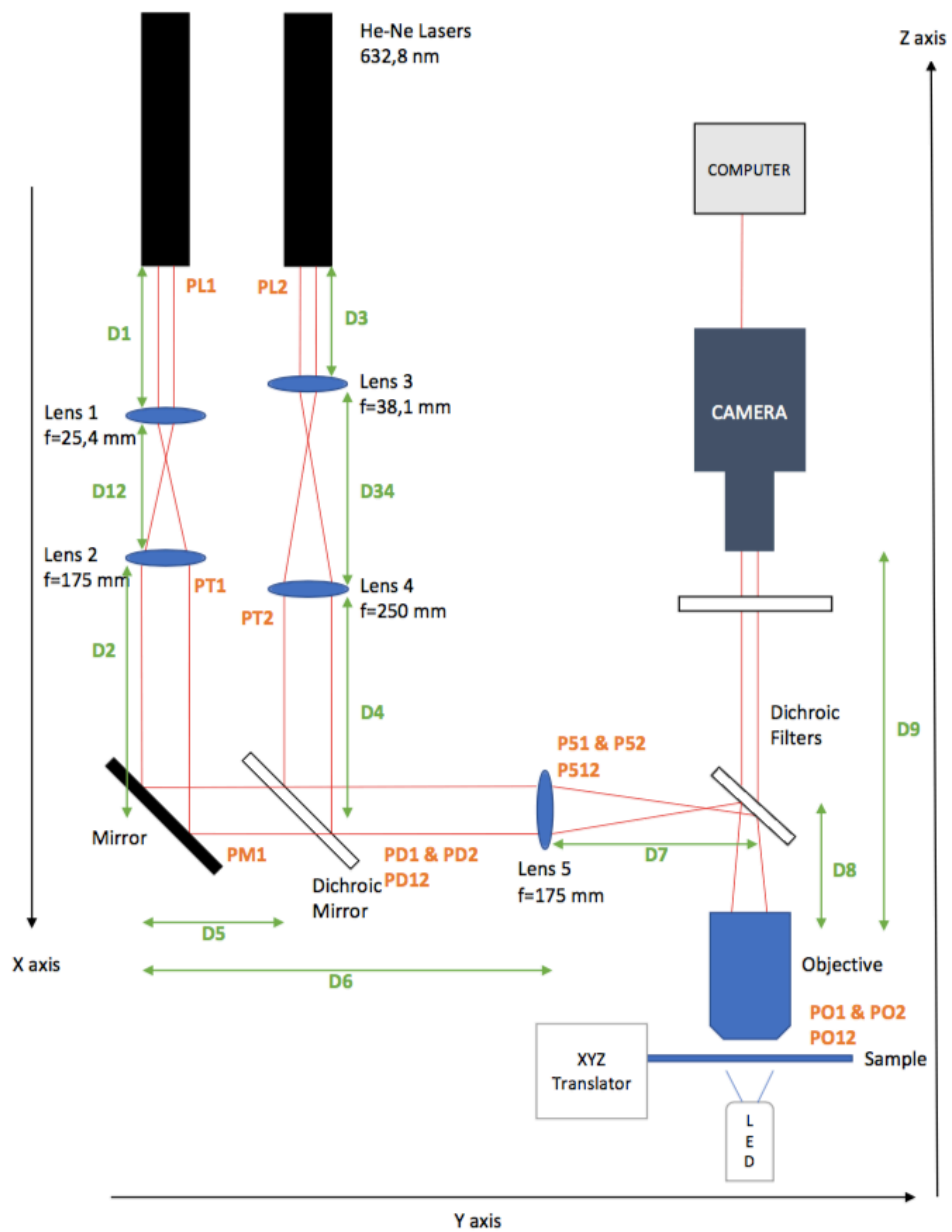
Figure 5.1: The setup of optical tweezer with dimensions and powers.

Table 5.1: Distances between optical components.

D1	690 mm
D12	205 mm
D2	580 mm
D3	675 mm
D34	300 mm
D4	500 mm
D5	115 mm
D6	215 mm
D7	280 mm
D8	20 mm
D9	40 mm

Distances between optical components (Table 5.1) were measured for best trapping performance. And the powers of the laser beams after optical systems were determined by powermeter (Thorlabs PM100D) (Table 5.2).

Table 5.2: Power of the beams after optical components.

	LASER 1	LASER 2	LASER 1&2
Output of the laser	PL1=25,45 mW	PL2=24,43 mW	-
After Telescope	PT1=19,28 mW	PT2=19,23 mW	-
After Mirror	PM1=15,70 mW	-	-
After Dichroic Mirror	PD1= 5,98 mW	PD2= 7,13 mW	PD12= 12,55 mW
After Lens 5	P51= 5,33 mW	P52= 6,68 mW	P512=11,62 mW
After Objective	PO1= 1,33 mW	PO2= 1,69 mW	PO12= 2,36 mW

In MATLAB, beam waists and radius of curvatures after telescopes and after lens L_5 were calculated by using ABCD matrix method for both lasers since the beam behaves as Gaussian beam (APPENDIX A). Beam waist after objective was determined at exit pupil and end of the working distance. Depth of focus was determined as 3 μm for both lasers. Beam waists after telescope system were determined as 4.82 mm and 4.60 mm for laser 1 and laser 2, respectively (Figure 5.2 and Figure 5.3).
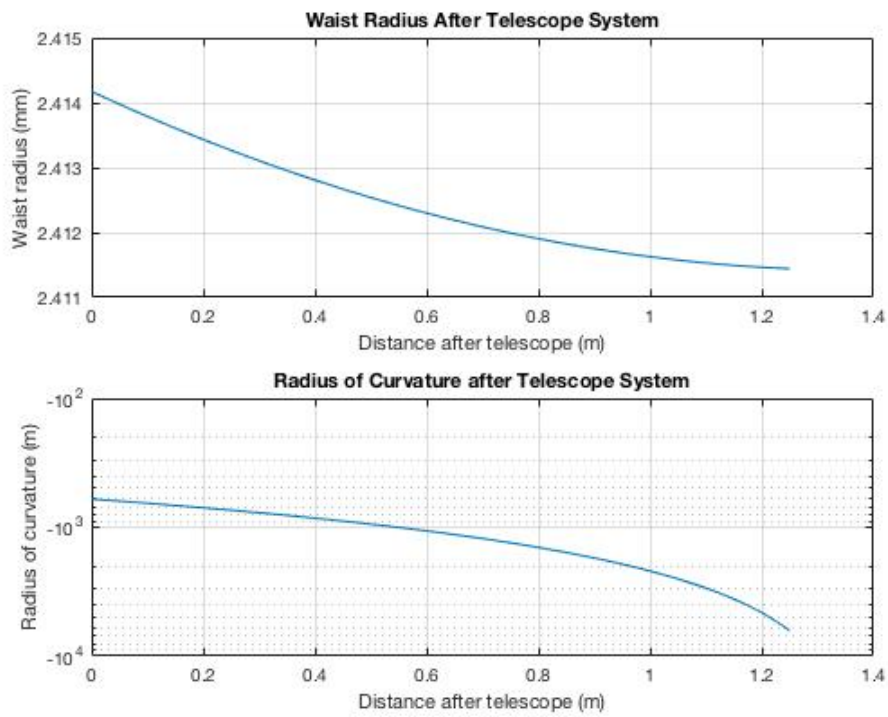
Figure 5.2: Waist radius and radius of curvature after telescope system for laser 1.
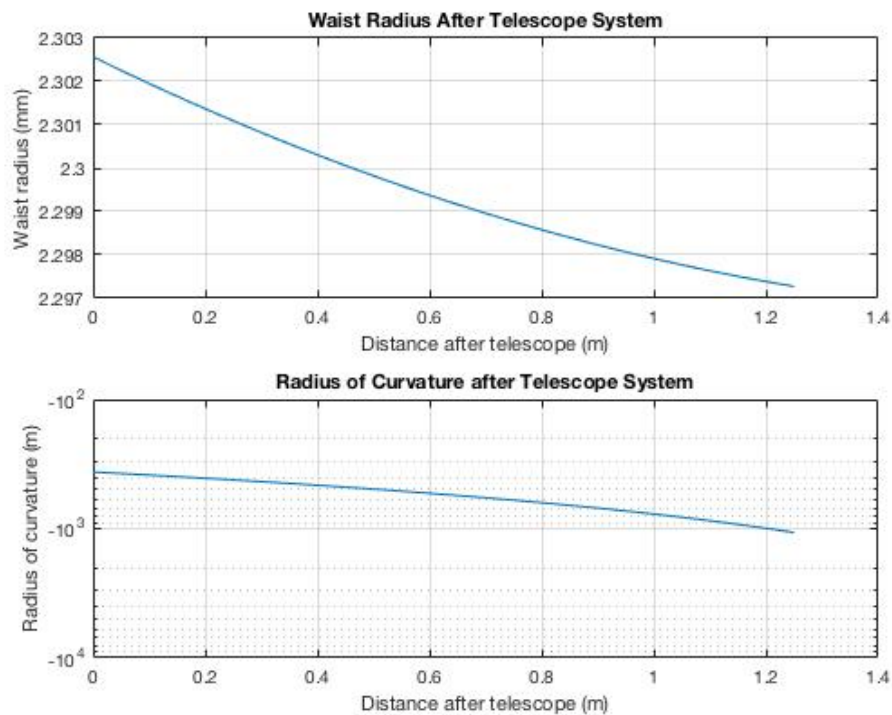
Figure 5.3: Waist radius and radius of curvature after telescope system for laser 2.

After lens 5, the minimum value of beam waist was calculated as 0.015 mm for both lasers. (Figure 5.4 and Figure 5.5). In experiments, objective located 300 mm after lens 5. And at this point beam waist was calculated as 1.732 mm and 1.652 mm for laser 1 and laser 2, respectively. In order to make beam diameter equal to objective diameter the distance between objective and lens 5 must be 353 mm for laser 1 and 373 mm for laser 2. However, in experiments the beam diameter equalled to objective diameter for both lasers.

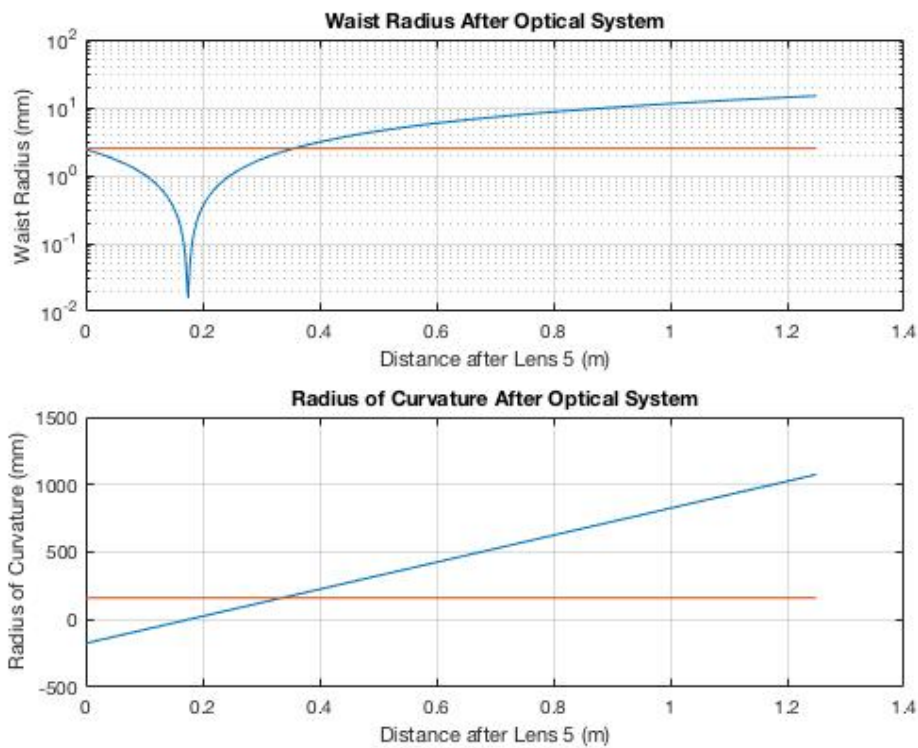**Figure 5.4:** Waist radius and radius of curvature after lens 5 for laser 1.
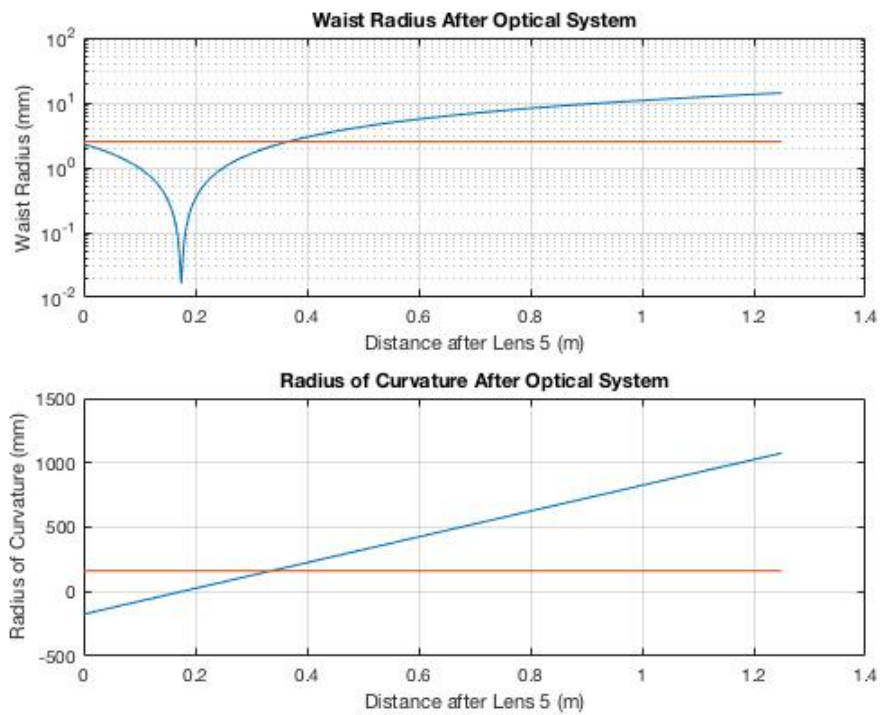
Figure 5.5: Waist radius and radius of curvature after lens 5 for laser 2.

Beam waist after objective was calculated as 17.23 µm and 16.44 µm at exit pupil for laser 1 and laser 2, respectively (Figure 5.6 and Figure 5.7).
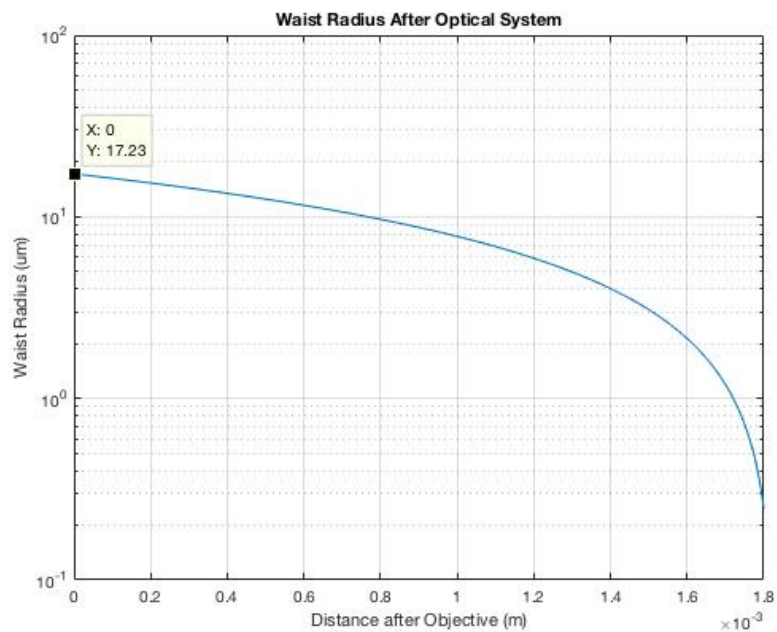
Figure 5.6: Waist radius after objective for laser 1.
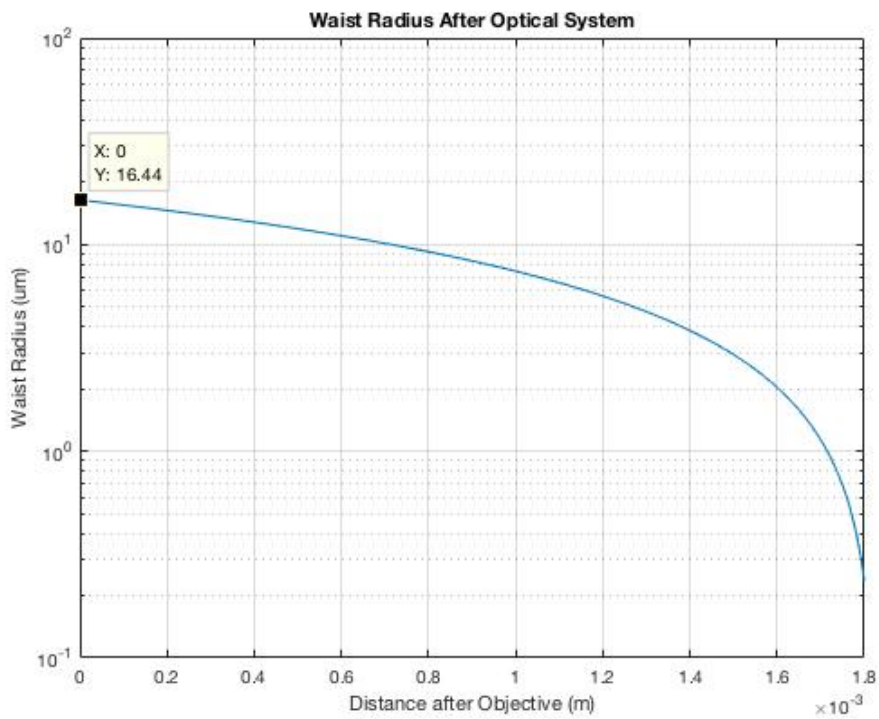
Figure 5.7: Waist radius after objective for laser 2.

In the experiments two lasers were located parallel to each other (Figure 5.8) and after reflecting mirrors they propagate closely to each other to the objective (Figure 5.9).
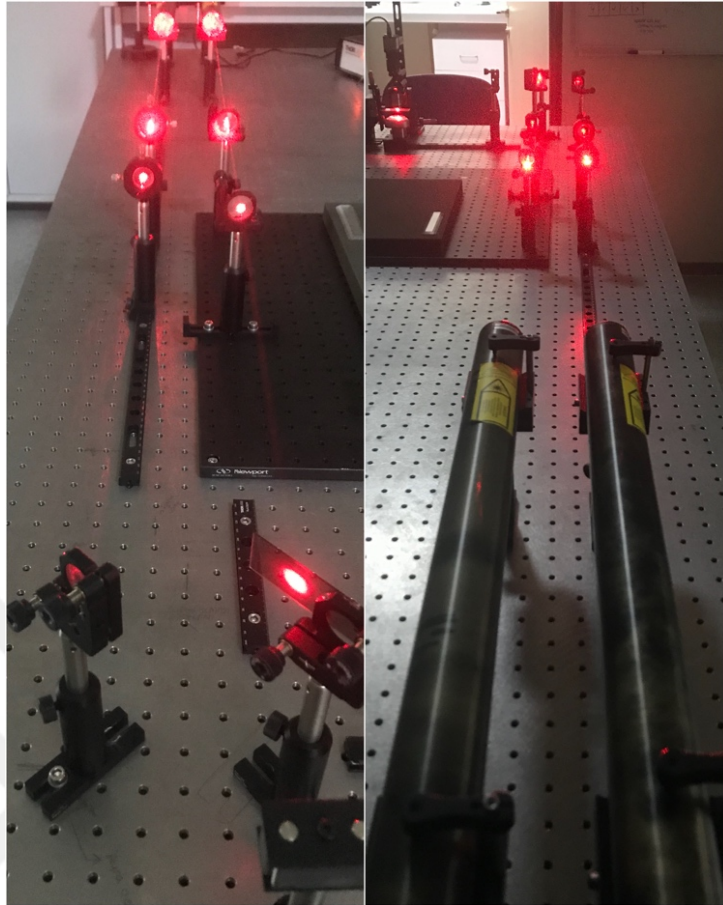
Figure 5.8: Views of telescopes and lasers in optical tweezer setup.
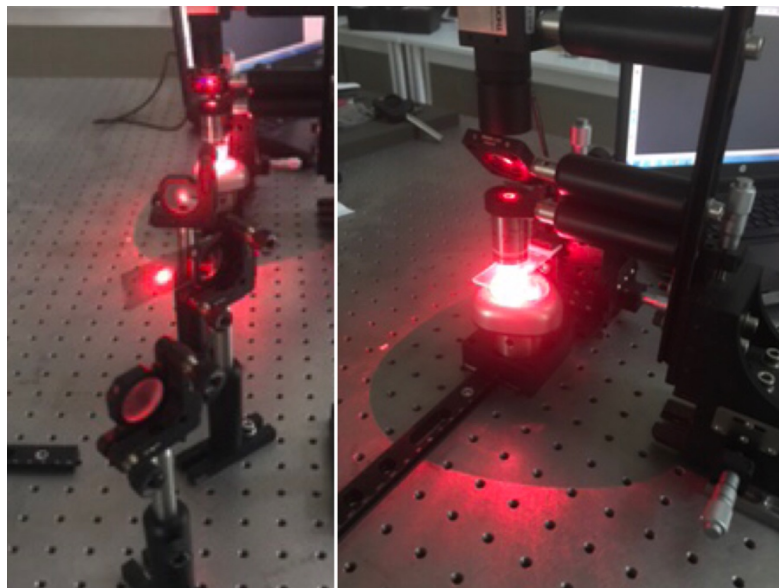
Figure 5.9: Views of the mirrors and objective in optical tweezer setup.

6. RESULTS

The stiffness and trapping force of optical tweezers were calculated by Brownian Motion method and drag force method. During experiments, absolute temperature was 23ºC. Uncertainities were related to change of temperature due to laser which is ±1.15 K and displacement which is ±0.005 μm.

According to Brownian Motion method, displacements of trapped particle must be measured to calculate $\langle x^2 \rangle$ in equations (6.1) and (6.2) [102]. Displacements of the trapped beads under Brownian Motion was determined by using ImageJ [103]. In order to determine displacements in μm-sized range, pixels converted to μm by measuring diameter of polystyrene bead. 1 μm equals to 48.11 pixels.

$$\langle x^2 \rangle = \frac{\sum_{n=1}^{N} x_n^2}{N} \tag{6.1}$$

$$\langle y^2 \rangle = \frac{\sum_{n=1}^{N} y_n^2}{N} \tag{6.2}$$

After finding displacements, the stiffnesses in both axis were calculated with equation (6.3) and (6.4).

$$\frac{1}{2} k_b T = \frac{1}{2} k \langle x^2 \rangle \tag{6.3}$$

$$\frac{1}{2} k_b T = \frac{1}{2} k \langle y^2 \rangle \tag{6.4}$$

Trapping force was found out by multiplication of stiffness (k) and distance of the bead's center from trap center, x.

$$F_T = kx \tag{6.5}$$

In order to find trapping force which equals to drag force in yeast cells, viscosity of fluid (μ), particle diameter (a) and velocity of fluid (v) must be known. Velocity of the fluid was measured by displacement of the reference point at a given time.

$$F_T = F_d = 6\pi\mu a v \tag{6.6}$$

And stiffness found out by equation (6.7)

$$k = \frac{F_T}{x} \qquad (6.5)$$

6.1 Characteristics of Optical Tweezer

The stiffness of optical tweezer and trapping force on polystyrene beads were calculated by using only Brownian Motion method since the particles inside fluid almost stayed still and drag force could not be measured in fluid due to low velocity of fluid. But polystyrene beads which were approximately 1μm were trapped and manipulated in water.

In order to calculate the stiffnesses and trapping forces of optical tweezers for x and y axis, polystyrene beads were trapped by Laser 1, Laser 2 and both lasers simultaneously. Contrast was added to pictures to show the trapped and moving particles.

6.1.1 Results of laser 1

Displacements were calculated by splitting of video to frames (Figure 6.1). Video of 3 seconds was splitted to 32 frames. Displacements were calculated by using equations (6.1) and (6.2) and they were found that $\langle x^2 \rangle$ equals to 2.108×10^{-16} m^2 and $\langle y^2 \rangle$ equals to 3.206×10^{-16} m^2.

According to equations (6.3) and (6.4), stiffnesses in both axis were found out as $k_x = 19.401 \pm 2.302$ pN/μm and $k_y = 12.754 \pm 0.996$ pN/μm.

The distance between trap center and center of the bead were 0.03 and 0.05 μm for x and y axis, respectively. Trapping force on polystyrene beads were found as $F_x = 0.582 \pm 0.070$ pN and $F_y = 0.637 \pm 0.050$ pN in both axis.

(a) **(b)**
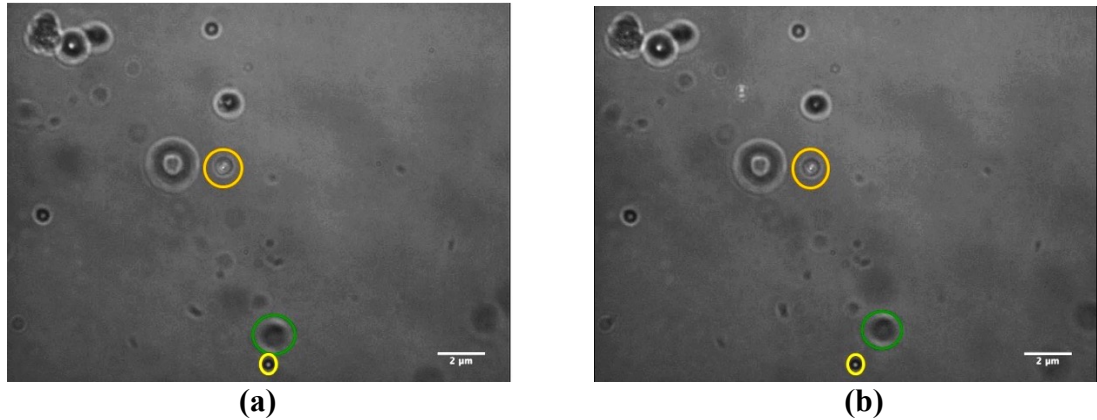
Figure 6.1: Trapped polystyrene bead by laser 1. The trapped polystyrene beads
were shown in orange circle. The particle which is in green circle was moving while
the bead in yellow circle was staying still at a given time. The (a) shows that at the
beginning of the trap, and (b) shows that end of the 3 seconds.

6.1.2 Results for Laser 2

Displacements were calculated by splitting of video to frames. Video of 1.8 seconds
was splitted to 20 frames (Figure 6.2). $\langle x^2 \rangle$ calculated as 4.738×10^{-16} m^2 and
$\langle y^2 \rangle$ equals to 4.034×10^{-16} m^2 according to equations (6.1) and (6.2). According to
equations (6.3) and (6.4), stiffnesses in both axis were found out as
$k_x = 8.623 \pm 0.457$ pN/μm and $k_y = 10.137 \pm 0.630$ pN/μm.

The distance between trap center and center of the bead were 0.03 and 0.04 μm for x
and y axis, respectively. Trapping force on polystyrene beads were found that F_x
equals to 0.259 ± 0.0144 pN and F_y equals to 0.405 ± 0.0257 pN in both axis.
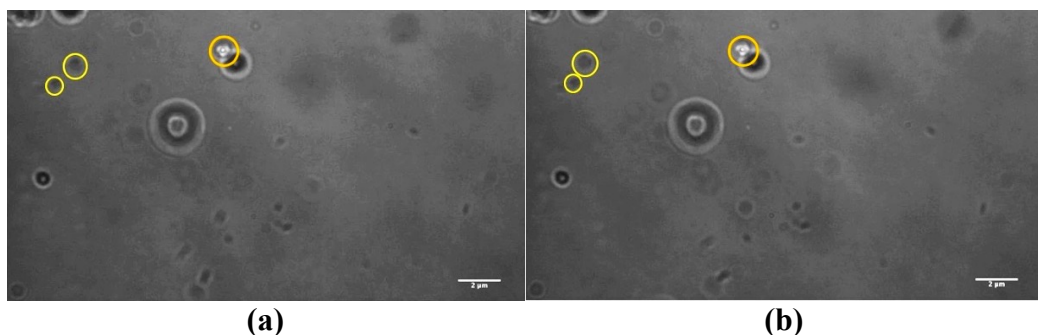

(a) **(b)**

Figure 6.2: Trapped polystyrene bead by laser 2. The trapped polystyrene beads
shown in orange circle. It is shown that the particles which are in yellow circle was
moving due to the fluid flow. The (a) shows that at the beginning of the trap, and (b)
shows that end of the 1.8 seconds.

6.1.3 Result when both lasers used simultaneously

The polystyrene beads trapped by both lasers when they used simultaneously (Figure 6.3). In order to find the displacements of the polystyrene beads, video of 1,25 seconds was splitted to 15 frames. $\langle x^2 \rangle$ calculated as 1.764×10^{-16} m^2 and $\langle y^2 \rangle$ equals to 3.585×10^{-16} m^2 according to equations (6.1) and (6.2). Stiffnesses in both axis were found out as $k_x = 23.179 \pm 3.290$ pN/μm and $k_y = 11.406 \pm 0.797$ pN/μm.

The distance between trap center and center of the bead were 0,01 μm for both x and y axis. Trapping force on polystyrene beads were found that F_x equals to $0,232 \pm 0,0349$ pN and F_y equals to $0,114 \pm 0,0098$ pN.

(a) (b)
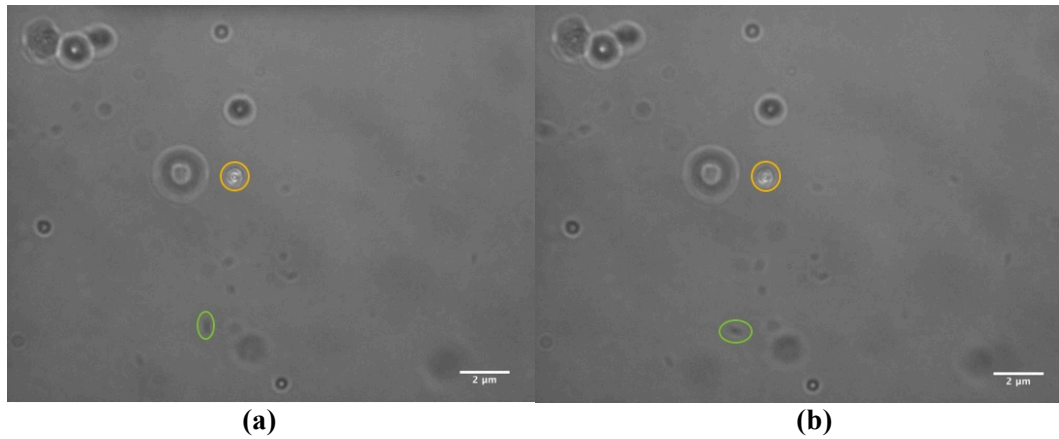
Figure 6.3: Trapped polystyrene bead by both lasers simultaneously. The trapped polystyrene beads shown in orange circle by both lasers simultaneously. It is shown that the particle which is in green circle was rotated at a given time. The (a) shows that at the beginning of the trap, and (b) shows that end of the 1.25 seconds.

6.1.4 Moving polystyrene beads with laser 2 to laser 1

Polystyrene bead was trapped and moved by laser 2 to laser 1. And then laser 1 trapped this particle (Figure 6.4). By this way, optical tweezer can be used in drug delivery applications.
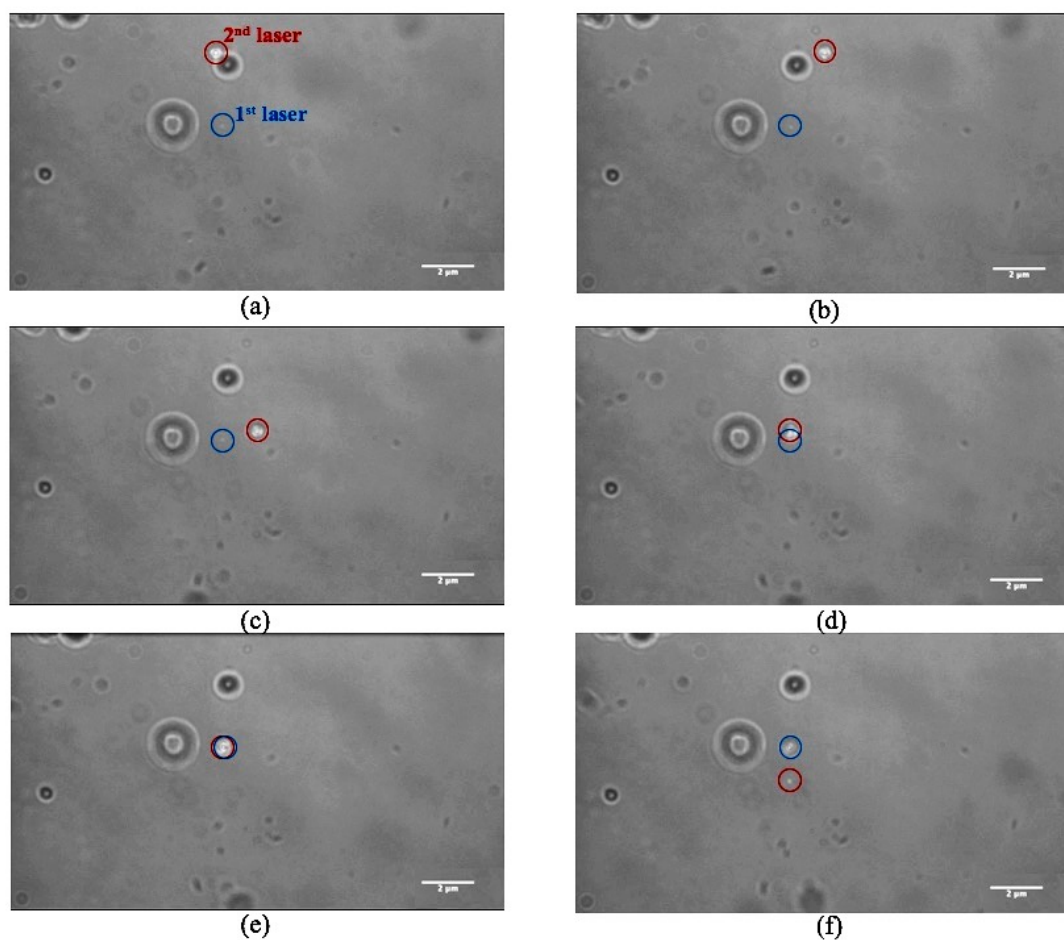
Figure 6.4: Moving polystyrene particles. the trapped polystyrene beads by laser 2 shown in red circle. The (a) shows that at the beginning of the trap, at (e) two lasers trapped the bead simultaneously and at (f) only laser 1 trapped the bead at 2 seconds.

6.1.5 Trapping multiple polystyrene beads

Optical tweezer is able to trap multiple polystyrene beads. The polystyrene bead was trapped by laser 2 and moved to laser 1. Laser 1 trapped this moved particle while it was trapping the other multiple particles (Figure 6.5).
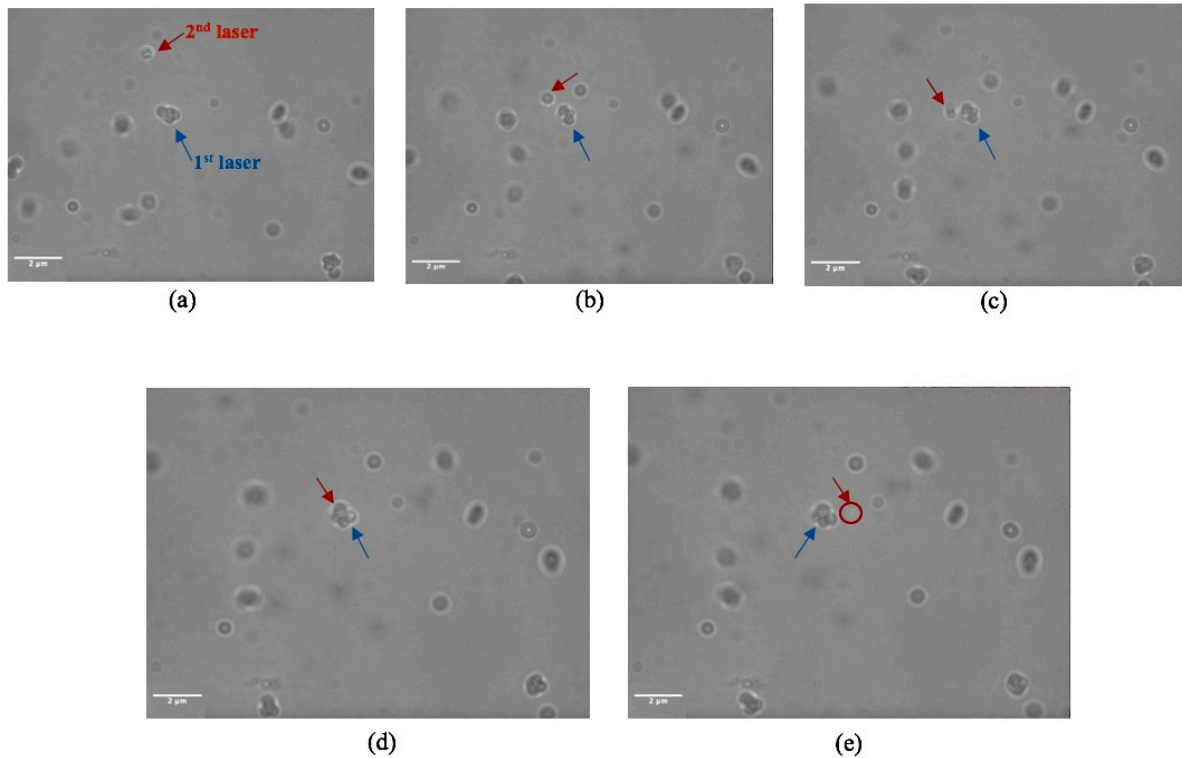
Figure 6.5: Trapping multiple particles. The polystyrene particle is trapped by laser 2 and moves to laser 1 in Figure 6.5 (a-c). At (d), laser 2 leaving the bead to laser 1 and at (e) laser 2 saperated from trapping region.

6.1.6   Comparison of lasers

Stiffnesses and trapping forces according to Brownian motion results are different from each other. Stiffness of laser 1 in x-axis is greater then laser 2 since it traps better than laser 2. But when both lasers trapped simultaneously, the stiffness in x-axis is greatest. Stiffnesses in y-direction were close to each other (Figure 6.6).

When both lasers were used simultaneously, the difference between stiffnesses in x and y-axis could be caused by the shape of particle or the overlapping of the lasers. If the particle were ellipsoid, it makes greater stiffness in that direction. And if the lasers did not overlap in x direction, k_x would be greater than k_y.
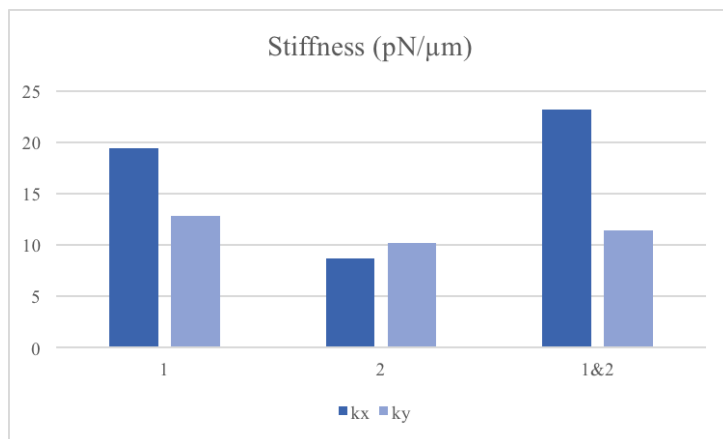
Figure 6.6: Stiffnesses of lasers.

The distance between trap center and center of the bead, x, is determinant of the trapping force. Increase in x results with greater forces to trap the particle. Therefore, Laser 1 has the greatest force in both axis (Figure 6.7). When both lasers were used simultaneously since the distance, x, was shorter than others the trapping force was less than others. And for laser 2, stiffnesses and trapping forces were in proportion.
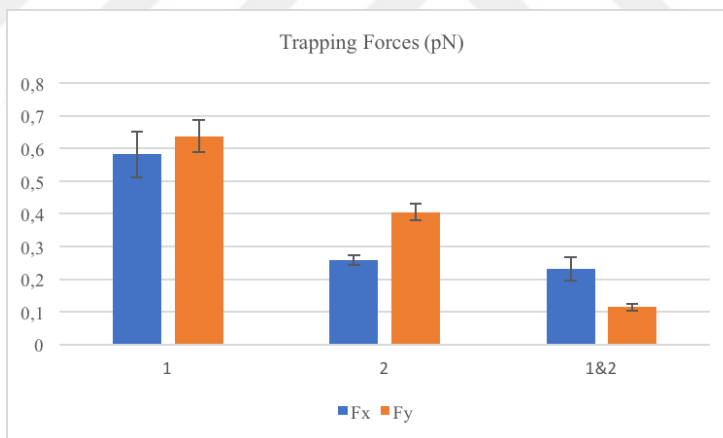
Figure 6.7: Trapping forces on the polystyrene beads.

6.2 Results for Yeast Cells

Stiffness and trapping force calculated by both Brownian Motion method and drag force method. Stiffnesses and trapping forces according to Brownian Motion were calculated as polystyrene beads.

In drag force method, 0.038 kg/ms was used as a viscosity of the yogurt culture [104]. The particle diameter measured for each calculation differently. In order to

calculate velocity of the fluid, the particle which had constant velocity was selected as a reference point.

Stiffness and trapping force were calculated by laser 1 and laser 2 in both axis. Uncertainities resulted from absolute temperature (1.150 K), displacement of reference point (0,500 μm), radius of beam (0.010 μm) and displacements for Brownian motion (1 nm).

6.2.1 Results for laser 1

In order to measure displacements of yeast cells in yogurt culture for Brownian Motion method, the video of 3 seconds was splitted to 30 frames (Figure 6.8). $\langle x^2 \rangle$ calculated as 7.056×10^{-16} m^2 and $\langle y^2 \rangle$ equals to 8.40533×10^{-16} m^2. Stiffnesses in both axis were found out as $k_x = 5.795 \pm 0.023$ pN/μm and $k_y = 4.865 \pm 0.019$ pN/μm.

The distance between trap center and center of the bead were 0.050 μm and 0.040 μm for x and y axis, respectively. Trapping force on polystyrene beads were found that F_x equals to 0.290 ± 0.006 pN and F_y equals to 0.195 ± 0.005 pN by Brownian Motion method (Figure 6.9).

The velocity component of fluid was found as 1.4405 μm/s for x-axis and 0.45699 μm/s for y-axis by displacements in 3 seconds. Viscosity of the medium equals to 0.038 kg/ms. And radius of the trapped yeast cell is 0.305 μm. Drag force calculated as 0.315 ± 0.057 pN for x-axis and 0.099 ± 0.041 pN for y-axis.

The stiffness is calculated by drag force method as 6.294 ± 1.140 pN/μm for x-axis and 2.496 ± 1.501 pN/μm for y-axis (Figure 6.10).

<div align="center">(a)   (b)</div>
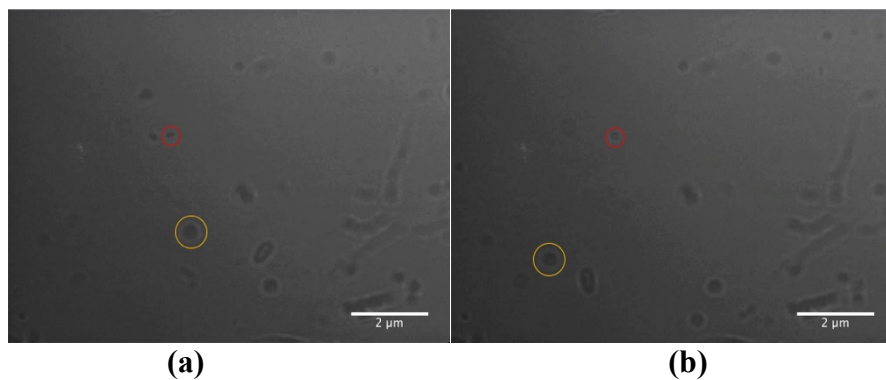
Figure 6.8: Trapping of yeast cells (Laser 1). The cell in yellow circle was moving while the yeast cell in red circle was trapping. (a) shows the beginning of the trap moment and (b) is the end of 3 seconds.
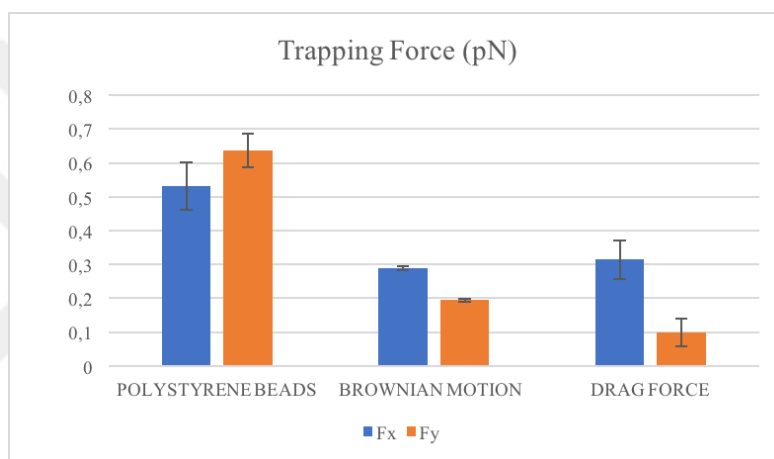
Figure 6.9: Comparison of trapping forces on the polystyrene beads and yeast cells (Laser 1).
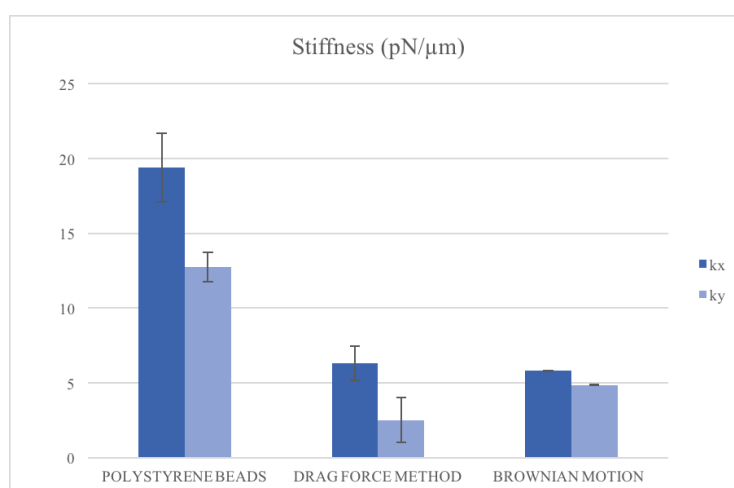
Figure 6.10: Comparison of stiffnesses for the polystyrene beads and yeast cells (Laser 1).

When the results of polystyrene beads are compared with results of yeast cells for laser 1, it is shown that there is a reduction in stiffness and trapping force values. It has been showed that the trapping forces in x-axis on yeast cells are close to each other but less than trapping force on polystyrene beads. It can be resulted from the viscosity or refractive index of the medium.

Reduction in stiffness for Brownian Motion can be caused by the displacement of the particle. Increase in displacement makes reduction in stiffness.

6.2.2 Results for laser 2

In order to measure displacements of yeast cells in yogurt culture for Brownian Motion method, the video of 1.9 seconds was splitted to 21 frames (Figure 6.11). $\langle x^2 \rangle$ calculated as 14.721×10^{-16} m^2 and $\langle y^2 \rangle$ equals to 9.391×10^{-16} m^2. Stiffnesses were found out as $k_x = 2.777 \pm 0.005$ pN/µm and $k_y = 4.354 \pm 0.117$ pN/µm for laser 2.

Trapping force on polystyrene beads were found that F_x equals to 0.139 ± 0.004 pN and F_y equals to 0.174 ± 0.006 pN by Brownian Motion method. And the distances between trap center and center of the bead were 0.05 µm and 0.04 µm for x and y axis, respectively.

The velocity component of fluid was found as 2.45 µm/s for x-axis and 0.467 µm/s for y-axis by displacements in 1.9 seconds. According to viscosity of 0.038 kg/ms and particle radius 0.5 µm, drag force calculated as 0.878 ± 0.150 pN for x-axis and 0.167 ± 0.097 pN for y-axis. The stiffness is calculated by drag force method as 14.627 ± 2.501 pN/µm for x-axis and 0.796 ± 0.461 pN/µm for y-axis.

(a)   (b)
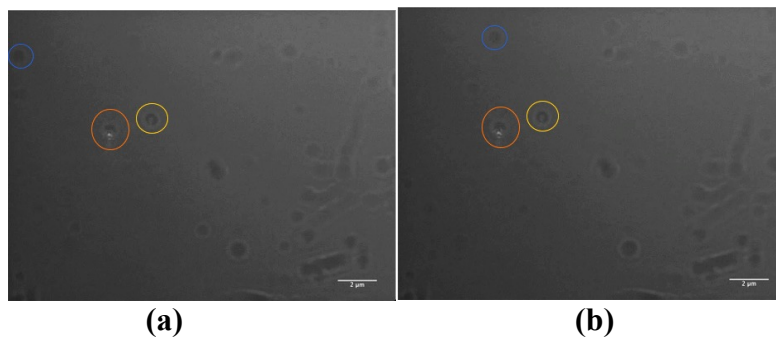
Figure 6.11: Trapping yeast cells (Laser 2). Trapped yeast cell by laser 2 is shown in orange circle and trapped yeast cell by laser 1 is shown in yellow circle. The cell in blue circle was moving while others trapping. (a) indicates the beginning of the trap and (b) indicates the end of the 1.9 seconds.

The stiffness and force values of polystyrene beads are greater than yeast cells in Brownian motion (Figure 6.12 and Figure 6.13). It is resulted from the displacement of the particles under Brownian Motion. Due to the fluid flow in x-axis stiffness and trapping force for drag force method is greater than values in y-axis.
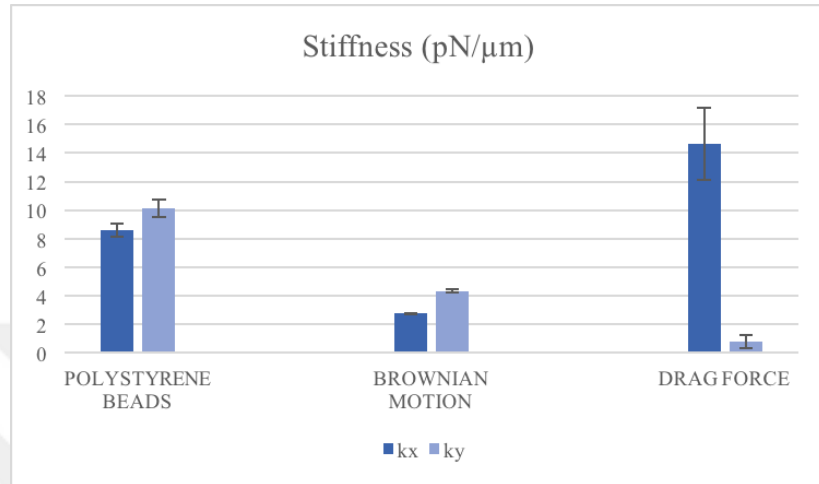
Figure 6.12: Comparison of stiffness for the polystyrene beads and yeast cells (Laser 2).
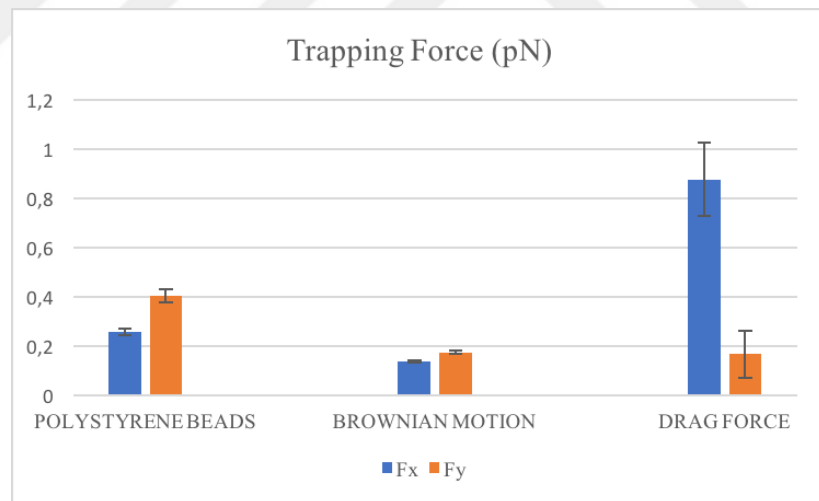
Figure 6.13: Comparison of trapping forces on the polystyrene beads and yeast cells (Laser 2).

6.2.3   Trapping multiple particles

Yeast cell was trapped and moved to laser 1 trapping region while laser 1 was trapping multiple yeast cells (Figure 6.14). The multiple yeast cells trapped by laser 1 and the yeast cell trapped and moved by laser 2.
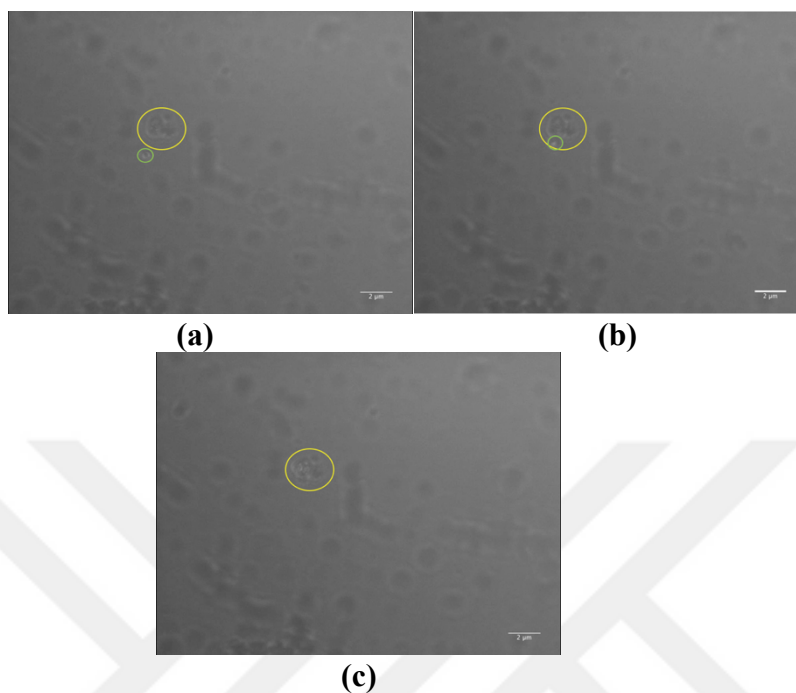
Figure 6.14: Trapping multiple yeast cells. (a) and (b) show that movement of trapped yeast cell in green circle by laser 2. (c) shows that trapping multiple cells which are in yellow circle by both lasers simultaneously.

6.2.4 Moving particle between each other

Laser 2 could trap yeast cell and leave it into trapping region of laser 1 (Figure 6.15).
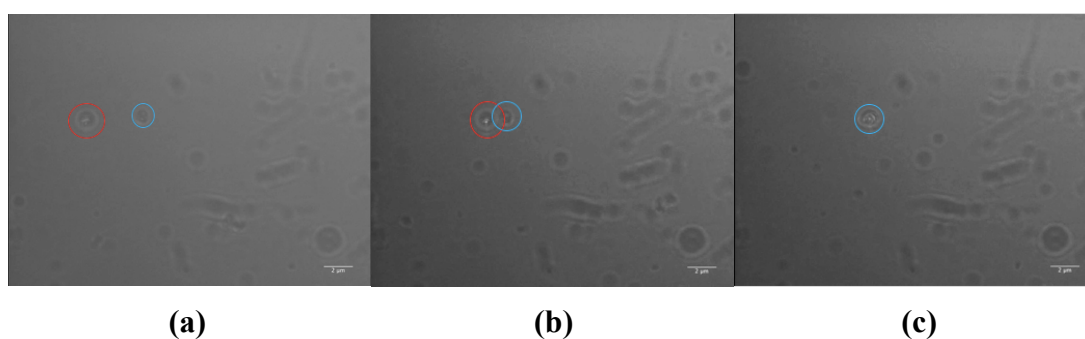
Figure 6.15: Trapping multiple yeast cells. Trapped yeast cells is shown in red circle (a-b) and in (c) yeast cells trapped by both lasers simultaneously.

6.3 Measuring Viscosity

Viscosity measurements of the yogurt culture medium was calculated by assuming that the stiffness of optical tweezer equals to polystyrene beads and trapping force on yeast cells equals to optical tweezers' trapping force which was characterized by using polystyrene beads.

Viscosity of medium contained yeast cells was calculated as 0.054±0.016 kg/ms for laser 1. For laser 2, viscosity of medium was calculated as 0.033±0.014 kg/ms.

Viscosity depends on the serum seperation of the yogurt culture. It has been showed that it varies 0.038-0.292 kg/ms under acoustic energy [104]. The yogurt culture medium used in experiments with laser 1 was favorable with the literature. The density of the yogurt culture has been defined 1.020 g/mL [105]. Reynolds number was calculated as 3.373×10^{-11} for laser 1 and 1.367×10^{-10} for laser 2. Small Reynolds number means that the fluid field is predictable and stable, viscous and surfaces forces dominates the fluid flow.

6.4 Results When Cytoplasmic Medium Was Used

The trapping force and stiffness were calculated theoretically by assuming the medium is cytoplasm of cells. Velocity and radius of yeast cells in calculations were assumed as values of yogurt culture. As a cytoplasm for calculations cytoplasm of *Schizosaccharomyces pombe* strain SP837 was used. *Schizosaccharomyces pombe* is called as "fission yeast". The apparent viscosity of the cytoplasm was measured between 0.1 to 0.8 Pa.s. Sacconi *et al.* have been measured the trapping force between 10-60 pN for viscosities in range of 0.1 to 0.8 Pa.s. But the results were doubtful since cytoplasm was inhomogoneous, viscoelestic and not purely viscous. And Stoke's law assumption of an infinite medium did not hold in cell surrounded by the stiff wall [30]. But in here, it is theoretically approximation of the application of this tweezer in cell medium. And the results were not different from the results in Sacconi *et al.*

If the cytoplasmic medium was used in experiments for laser 1, trapping force and stiffness differ due to the viscosity (Figure 6.16 and Figure 6.17). X-axis component

of trapping force was changed from 0.828±0.132 pN to 6.625±0.828 pN. And y component of the trapping force varied between 0.263±0.106 pN and 2.102±0.824 pN.

Stiffnesses were calculated for both axis. k_x varied between 16.563±2.664 pN/μm and 132.505±16.778 pN/μm. k_y was in the range of 6.568±3.345 pN/μm and 52.546±20.658 pN/μm.
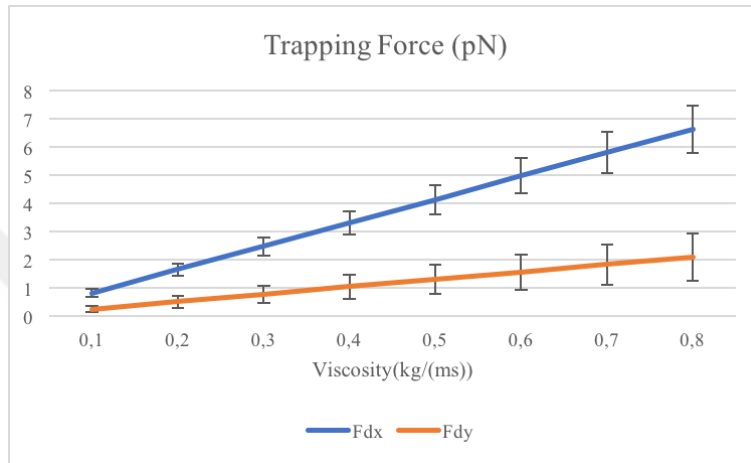
Figure 6.16: Trapping force for cytoplasmic medium (Laser 1).
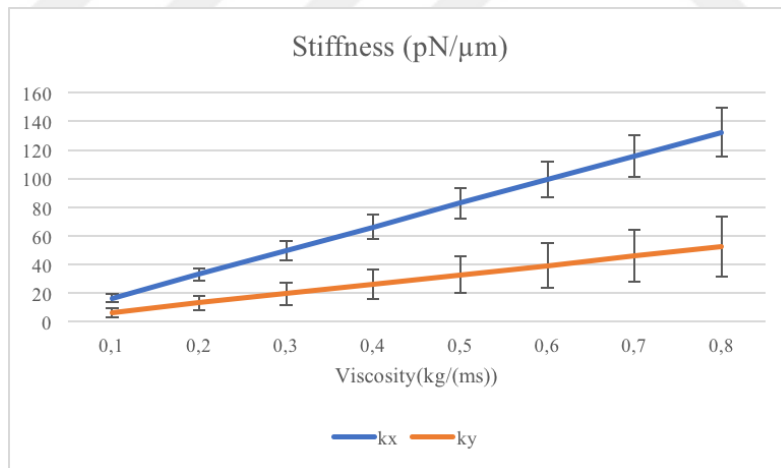
Figure 6.17: Stiffness for cytoplasmic medium (Laser 1).

Stiffness and trapping force were directly propotional to viscosity since the velocity was constant. But in reality, the velocity depends upon the viscosity. Therefore, the plots can be changed. But the trapping forces in these range has been appropriate to results of Sacconi *et al*. Forces at low viscosities has been smaller than results of Sacconi *et al.* due to the velocity.

All calculations about stiffness and trapping force in cytoplasmic medium were applied for laser 2 (Figure 6.18 and Figure 6.19). Stiffness changed between 38.493±4.253 pN/μm and 307.942±34.027 pN/μm for x-axis. And stiffness in y-axis varied in the range of 2.095±1.182 pN/μm and 16.761±9.454 pN/μm.

Component of trapping force in x-axis was changed from 2.310±0.252 pN to 18.476±2.180 pN. And component in y-axis varied between 0.440±0.248 pN and 3.520±1.985 pN.
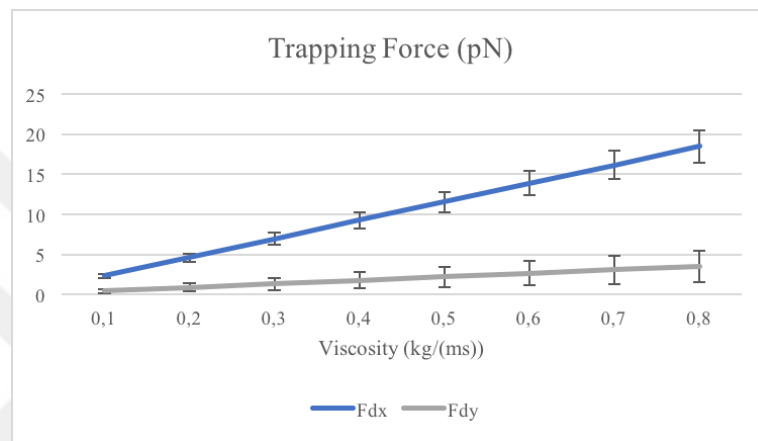
Figure 6.18: Trapping force for cytoplasmic medium (Laser 2).
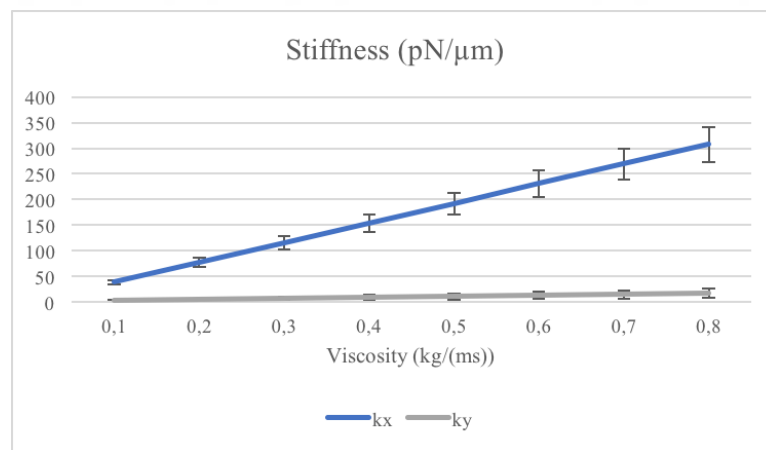
Figure 6.19: Stiffness for cytoplasmic medium (Laser 2).

Stiffness of laser 2 are shown as greater than laser 1 (Figure 6.19). It was resulted from the velocity of the fluid. Although the trapping forces is favorable with the results of Sacconi *et al* [30].

6.5 Trapping Efficiency of the System

Trapping efficiency of the system was calculated for both yeast cells in yogurt culture and polystyrene beads in water for each condition (Figure 6.20). Trapping efficiency was determined by Q=Fc/nP equation. F is the trapping force, P is the trapping power, c is the speed of the light and n is the refractive index of the medium. In order to calculate the trapping efficiency, as a trapping force found out by Brownian motion method was used. Refractive index of medium was 1.330 for water and 1.352 for yogurt culture [106]. Efficiency had the maximum value for trapped polystyrene beads by laser 1. When both lasers used simultaneously, efficiency had minimum value since laser beams could not overlapped and it effected the trapping force. Efficiencies of yeast cells was calculated lower than polystyrene beads due to refractive index of the medium.
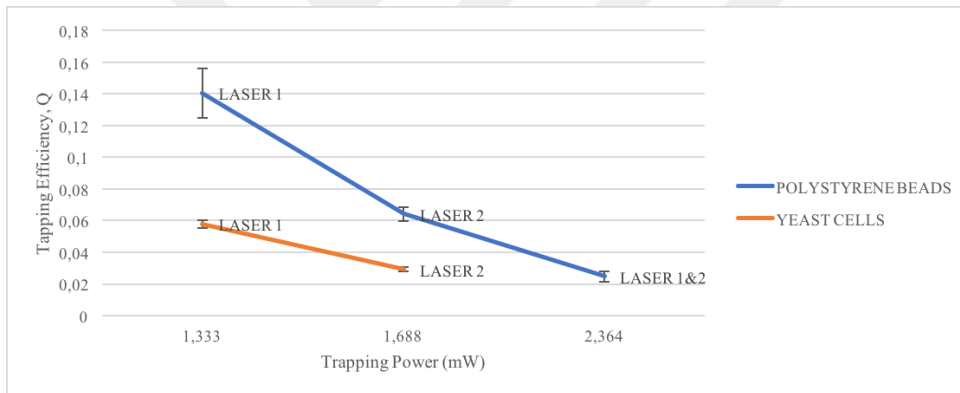
Figure 6.20: Trapping efficiencies.

Trapping efficiencies (Q) of polystyrene beads calculated as 0.140±0.015, 0.064±0.004, 0.025±0.004 for laser 1, laser 2 and both lasers used simultaneously. And for yeast cells they were calculated as 0.058±0.003 and 0.029±0.001 for laser 1 and laser 2, respectively.

Trapping efficiency was calculated also for yeast cells in cytoplasmic medium. The refractive index cytoplasmic medium was determined as 1.393±0.006 [107]. Trapping efficiency of this optical tweezer in trapping yeast cells in cytoplasmic medium 0.1403±0.027 for laser 1 and 0.300±0.046 for laser 2. Trapping efficiencies in cytoplasmic medium were greater than in water or yogurt culture since the trapping force due is greater due to viscosity of the medium.

7. CONCLUSIONS

The aim of this thesis was trapping yeast cells with custom designed optical tweezer which uses two He-Ne lasers (λ=632.8 nm) parallel to each other. Optical tweezers use the forces of laser radiation pressure to trap and manipulate microscopic particles. The stiffness and the trapping force of optical tweezer was determined by using Brownian Motion and Drag Force methods in order to characterize the specs of the original setup and its potential applications in life science. Characteristic specs for polystyrene beads were determined only Brownian Motion method since low velocity of fluid hindered the calibration with Drag Force Method. Stiffnesses and trapping forces of optical tweezer for each condition (Laser 1, Laser 2 and when both lasers were used simultaneously) were calculated and compared with results of yeast cells. The stiffness depended on the shape of the particle since stiffness in x-direction was dfferent from stiffness in y-direction. This optical tweezer system can trap multiple polystyrene beads and yeast cells and laser 2 can move particle (polystyrene beads or yeast cells) to laser 1 while laser 1 is trapping other particles. In contrary to polystyrene beads, stiffness and trapping force values of yeast cells in yogurt culture decreased due to refractive index of particle and viscosity of fluid. For laser 2 drag force in x-direction was greater than other forces since reference particle had high velocity in x-direction. Viscosity of yogurt culture found as quantitatively applicable with the results in the literature [104]. The serum seperation of yogurt affects to the viscosity of the yogurt drink. The applicability of this optical setup inside yeast cell was studied by calculating the trapping force. Trapping force created by custom designed optical tweezer was favorable with the results [30]. At lower viscosities, the trapping force is less then results of Sacconi *et al*. since the velocity of fluid is lower. Optical tweezer trapping polystrene beads in water has greater efficiency than yeast cells in yogurt culture. Trapping efficiency of optical tweezer had the highest value for the cytoplasmic medium since the high viscostiy of medium affected the trapping

force positively. By this way, the optical tweezer which is applicable inside yeast cell was designed theoretically.

REFERENCES

[1] **Ashkin, A.** (1970). Acceleration and Trapping of Particles by Radiation Pressure, *Physical Review Letters*, *24*(4), 156–159. https://doi.org/10.1103/PhysRevLett.24.156

[2] **Ashkin, A., Dziedzic, J. M., Bjorkholm, J. E., & Chu, S.** (1986). Observation of a single-beam gradient force optical trap for dielectric particles, *Optics Letters*, *11*(5), 288. https://doi.org/10.1364/OL.11.000288

[3] **Ashkin, A., & Dziedzic, J. M.** (1987). Optical trapping and manipulation of viruses and bacteria, *Science*, *235*(1984), 1517–1520. https://doi.org/10.1126/science.3547653

[4] **Lang, M. J., & Block, S. M.** (2003). Resource Letter: LBOT-1: Laser-based optical tweezers, *American Journal of Physics*, *71*(3), 201–215.

[5] **Mas Soler, J.** (2008). *Force calibration of optical traps by video-based methods* (Master's thesis). Retrieved from http://upcommons.upc.edu/bitstream/handle/2099.1/6013/MSc_in_Photonics _Thesis_Josep_Mas.pdf;jsessionid=817869C61134B5F0AD31B40D789E909 1?sequence=1

[6] **Kappel, K., & Lind, C. H.** (2014). Trapping Polystyrene Beads with Optical Tweezers,.

[7] **Rice, A., & Fischer, R.** (n.d.) *Calibration Of Optical Tweezers*. Eugene, OR.

[8] **Baek, J.-H., Hwang, S.-U., & Lee, Y.-G.** (2007). Trap stiffness in optical tweezers, In *Asian Symposium for Precision Engineering and Nanotechnology 2007* (p. 6).

[9] **Maxwell, J. C.** (1873). A treatise on electricity and magnetism Vol.II, *Oxford: Clarendon Press*. https://doi.org/10.1016/0016-0032(54)90053-8

[10] **Padgett, M. J., Molloy, J., & McGloin, D.** (2010). *Optical Tweezers: Methods and Applications*. CRC Press. Retrieved from https://books.google.com.tr/books?id=KynNBQAAQBAJ

[11] **Bartoli, A.** (1884). Il calorico raggiante e il secondo principio di termodinamica, *Il Nuovo Cimento (1877-1894)*, *15*(1), 193–202. https://doi.org/10.1007/BF02737234

[12] **Crookes, W.** (1874). On Attraction and Repulsion Resulting from Radiation, *Philosophical Transactions of the Royal Society of London*, *1*(1874), 501–527. https://doi.org/10.1017/CBO9781107415324.004

[13] **Nichols, E. F., & Hull, G. F.** (1901). A Preliminary Communication on the Pressure of Heat and Light Radiation, *Physical Review (Series I)*, *13*(5), 307–320. https://doi.org/doi: 10.1103/physrevseriesi.13.307

[14] **Lebedew, P.** (1901). Untersuchungen über die Druckkräfte des Lichtes, *Annalen Der Physik*, *311*(11), 433–458.

[15] **Nichols, E. F., & Hull, G. F.** (1903). The pressure due to radiation. (second paper.), *Physical Review (Series I)*, *17*(2), 91–104. https://doi.org/10.1103/PhysRevSeriesI.17.91

[16] **Ashkin, A., & Dziedzic, J. M.** (1971). Optical levitation by radiation pressure,

Applied Physics Letters, *19*(8), 283–285. https://doi.org/10.1063/1.1653919

[**17**] **Ashkin, A., & Dziedzic, J. M.** (1976). Optical levitation in high vacuum, *Applied Physics Letters*, *28*(6), 333–335. https://doi.org/10.1063/1.88748

[**18**] **Ashkin, A., & Dziedzic, J. M.** (1977). Feedback stabilization of optically levitated particles, *Applied Physics Letters*, *30*(4), 202–204. https://doi.org/10.1063/1.89335

[**19**] **Ashkin, A., & Dziedzic, J. M.** (1976). Observation of a new nonlinear photoelectric effect using optical levitation, *Physical Review Letters*, *36*(5), 267–270. https://doi.org/10.1103/PhysRevLett.36.267

[**20**] **Ashkin, A., & Dziedzic, J. M.** (1973). Radiation pressure on a free liquid surface, *Physical Review Letters*, *30*(4), 139–142. https://doi.org/10.1103/PhysRevLett.30.139

[**21**] **Ashkin, A., & Dziedzic, J. M.** (1975). Optical Levitation of Liquid Drops by Radiation Pressure, *Source: Science, New Series*, *187*(21), 1073–1075. https://doi.org/10.1126/science.187.4181.1073

[**22**] **Ashkin, A., & Dziedzic, J. M.** (1977). Observation of resonances in the radiation pressure on dielectric spheres, *Physical Review Letters*, *38*(23), 1351–1354. https://doi.org/10.1103/PhysRevLett.38.1351

[**23**] **Symes, R., Sayera, R. M., & Reid, J. P.** (2004). Cavity enhanced droplet spectroscopy: Principles, perspectives and prospects, *Phys. Chem. Chem. Phys.*, (6), 474–487. https://doi.org/10.1039/b313370b

[**24**] **Sayed, R.** (2017). Quantitative optical trapping and optical manipulation of micro-sized objects., *Semiconductor Physics, Quantum Electronics & Optoelectronics*, *20*(3), 349–354.

[**25**] **Andersson, M.** (2007). *Construction of force measuring optical tweezers instrumentation and investigations of biophysical properties of bacterial adhesion organelles* (Doctoral dissertion). Retrieved from https://arxiv.org/pdf/1503.00881.pdf

[**26**] **Thrasher, P. W.** (2011). *Measuring the nonconservative force field in an optical trap and imaging biopolymer networks with Brownian motion* (Doctoral Dissertion). Retrieved from https://repositories.lib.utexas.edu/handle/2152/20675

[**27**] **Berns, M. W., Wright, W. H., Tromberg, B. J., Profeta, G. A., Andrews, J. J., & Walter, R. J.** (1989). Use of a laser-induced optical force trap to study chromosome movement on the mitotic spindle, *Proceedings of the National Academy of Sciences*, *86*(12), 4539–4543.

[**28**] **Townes-Anderson, E., St Jules, R. S., Sherry, D. M., Lichtenberger, J., & Hassanain, M.** (1998). Micromanipulation of retinal neurons by optical tweezers, *Mol Vis*, *4*, 12.

[**29**] **Kulin, S., Kishore, R., Helmerson, K., & Locascio, L.** (2003). Optical manipulation and fusion of liposomes as microreactors, *Langmuir*, *19*(20), 8206–8210.

[**30**] **Sacconi, L., Tolić-Nørrelykke, I. M., Stringari, C., Antolini, R., & Pavone, F. S.** (2005). Optical micromanipulations inside yeast cells, *Applied Optics*, *44*(11), 2001–2007.

[**31**] **Zhong, M.-C., Wei, X.-B., Zhou, J.-H., Wang, Z.-Q., & Li, Y.-M.** (2013). Trapping red blood cells in living animals using optical tweezers, *Nature Communications*, *4*, 1768.

[32] **Johansen, P. L., Fenaroli, F., Evensen, L., Griffiths, G., & Koster, G.** (2016). Optical micromanipulation of nanoparticles and cells inside living zebrafish, *Nature Communications*, *7*, 10974.

[33] **Nemet, B. A., & Cronin-Golomb, M.** (2003). Measuring microscopic viscosity with optical tweezers as a confocal probe, *Applied Optics*, *42*(10), 1820–1832.

[34] **Statsenko, A., Inami, W., & Kawata, Y.** (2017). Measurement of viscosity of liquids using optical tweezers, *Optics Communications*, *402*, 9–13.

[35] **Eom, N., Stevens, V., Wedding, A. B., Sedev, R., & Connor, J. N.** (2014). Probing fluid flow using the force measurement capability of optical trapping, *Advanced Powder Technology*, *25*(4), 1249–1253.

[36] **Jing, P., Wu, J., Liu, G. W., Keeler, E. G., Pun, S. H., & Lin, L. Y.** (2016). Photonic crystal optical tweezers with high efficiency for live biological samples and viability characterization, *Scientific Reports*, *6*.

[37] **Shilkin, D. A., Lyubin, E. V, Soboleva, I. V, & Fedyanin, A. A.** (2014). Trap position control in the vicinity of reflecting surfaces in optical tweezers, *JETP Letters*, *98*(10), 644–647.

[38] **Kang, Z., Chen, J., Wu, S.-Y., Chen, K., Kong, S.-K., Yong, K.-T., & Ho, H.-P.** (2015). Trapping and assembling of particles and live cells on large-scale random gold nano-island substrates, *Scientific Reports*, *5*, 9978.

[39] **Svoboda, K., Schmidt, C. F., Schnapp, B. J., & Block, S. M.** (1993). Direct observation of kinesin stepping by optical trapping interferometry, *Nature*, *365*(6448), 721–727.

[40] **Block, S. M., Goldstein, L. S. B., & Schnapp, B. J.** (1990). Bead movement by single kinesin molecules studied with optical tweezers, *Nature*, *348*(6299), 348–352.

[41] **Smith, S. B., Cui, Y., & Bustamante, C.** (1996). Overstretching B-DNA: the elastic response of individual double-stranded and single-stranded DNA molecules, *Science*, 795–799.

[42] **Tsuda, Y., Yasutake, H., Ishijima, A., & Yanagida, T.** (1996). Torsional rigidity of single actin filaments and actin–actin bond breaking force under torsion measured directly by in vitro micromanipulation, *Proceedings of the National Academy of Sciences*, *93*(23), 12937–12942.

[43] **Khatibzadeh, N., Stilgoe, A. B., Bui, A. A. M., Rocha, Y., Cruz, G. M., Loke, V., … Berns, M. W.** (2014). Determination of motility forces on isolated chromosomes with laser tweezers, *Scientific Reports*, *4*.

[44] **Suei, S., Raudsepp, A., Kent, L. M., Keen, S. A. J., Filichev, V. V, & Williams, M. A. K.** (2015). DNA visualization in single molecule studies carried out with optical tweezers: Covalent versus non-covalent attachment of fluorophores, *Biochemical and Biophysical Research Communications*, *466*(2), 226–231.

[45] **Yethiraj, A.** (2007). Tunable colloids: control of colloidal phase transitions with tunable interactions, *Soft Matter*, *3*(9), 1099–1115.

[46] **Bar-Ziv, R., Frisch, T., & Moses, E.** (1995). Entropic expulsion in vesicles, *Physical Review Letters*, *75*(19), 3481.

[47] **Simon, A., & Libchaber, A.** (1992). Escape and synchronization of a Brownian particle, *Phys. Rev. Lett.*, *68*(23), 3375–3378. https://doi.org/10.1103/PhysRevLett.68.3375

[**48**] **Wang, G. M., Sevick, E. M., Mittag, E., Searles, D. J., & Evans, D. J.** (2002). Experimental Demonstration of Violations of the Second Law of Thermodynamics for Small Systems and Short Time Scales, *Phys. Rev. Lett.*, *89*(5), 50601. https://doi.org/10.1103/PhysRevLett.89.050601

[**49**] **Rubinsztein-Dunlop, H., Nieminen, T. A., Friese, M. E. J., & Heckenberg, N. R.** (1998). Optical trapping of absorbing particles, *Advances in Quantum Chemistry*, *30*, 469–492.

[**50**] **Svoboda, K., & Block, S. M.** (1994). Optical trapping of metallic Rayleigh particles, *Optics Letters*, *19*(13), 930–932.

[**51**] **Seol, Y., Carpenter, A. E., & Perkins, T. T.** (2006). Gold nanoparticles: enhanced optical trapping and sensitivity coupled with significant heating, *Optics Letters*, *31*(16), 2429–2431.

[**52**] **Hansen, P. M., Bhatia, V. K., Harrit, N., & Oddershede, L.** (2005). Expanding the optical trapping range of gold nanoparticles, *Nano Letters*, *5*(10), 1937–1942.

[**53**] **Jauffred, L., Richardson, A. C., & Oddershede, L. B.** (2008). Three-dimensional optical control of individual quantum dots, *Nano Letters*, *8*(10), 3376–3380.

[**54**] **Plewa, J., Tanner, E., Mueth, D. M., & Grier, D. G.** (2004). Processing carbon nanotubes with holographic optical tweezers, *Optics Express*, *12*(9), 1978–1981.

[**55**] **Bhatt, J., Kumar, A., Singh, R. P., & Jaaffrey, S. N. A.** (2015). Optical trapping of fluorescent beads, *Journal of Experimental Nanoscience*, *10*(4), 290–298.

[**56**] **Magazzú, A., Spadaro, D., Donato, M. G., Sayed, R., Messina, E., D'Andrea, C., … Maragó, O. M.** (2015). Optical tweezers: a non-destructive tool for soft and biomaterial investigations, *Rendiconti Lincei*, *26*(2), 203–218. https://doi.org/10.1007/s12210-015-0395-4

[**57**] **Li, T.** (2012). Physical Principles of Optical Tweezers, In *Fundamental Tests of Physics with Optically Trapped Microspheres* (pp. 9–21). Springer Science & Business Media. https://doi.org/10.1007/978-1-4614-6031-2

[**58**] **Ashkin, A.** (1992). Forces of a single-beam gradient laser trap on a dielectric sphere in the ray optics regime, *Biophysical Journal*, *61*(2), 569–582. https://doi.org/10.1016/S0006-3495(92)81860-X

[**59**] **Malagnino, N., Pesce, G., Sasso, A., & Arimondo, E.** (2002). Measurements of trapping efficiency and stiffness in optical tweezers, *214*, 15–24.

[**60**] **Zhang, H., & Liu, K.** (2008). Optical tweezers for single cells, *Journal of the Royal Society, Interface / the Royal Society*, *5*, 671–690. https://doi.org/10.1098/rsif.2008.0052

[**61**] **Lock, J. A., & Gouesbet, G.** (2009). Generalized Lorenz–Mie theory and applications, *Journal of Quantitative Spectroscopy and Radiative Transfer*, *110*(11), 800–807.

[**62**] **Davis, L. W.** (1979). Theory of electromagnetic beams, *Physical Review*, *19*(3), 1177.

[**63**] **Barton, J. P., & Alexander, D. R.** (1989). Fifth-order corrected electromagnetic field components for a fundamental Gaussian beam, *Journal of Applied Physics*, *66*(7), 2800–2802.

[**64**] **Gouesbet, G., Maheu, B., & Gréhan, G.** (1988). Light scattering from a sphere

arbitrarily located in a Gaussian beam, using a Bromwich formulation, *Journal of the Optical Society of America A*, *5*(9), 1427–1443. https://doi.org/10.1364/JOSAA.5.001427

[**65**] **Maheu, B., Gouesbet, G., & Gréhan, G.** (1988). A concise presentation of the generalized Lorenz-Mie theory for arbitrary location of the scatterer in an arbitrary incident profile, *Journal of Optics*, *19*(2), 59. Retrieved from http://stacks.iop.org/0150-536X/19/i=2/a=002

[**66**] **Barton, J. P., Alexander, D. R., & Schaub, S. A.** (1989). Theoretical determination of net radiation force and torque for a spherical particle illuminated by a focused laser beam, *Journal of Applied Physics*, *66*(10), 4594–4602.

[**67**] **Kim, J. S., & Lee, S. S.** (1983). Scattering of laser beams and the optical potential well for a homogeneous sphere, *JOSA*, *73*(3), 303–312.

[**68**] **Chang, S., & Lee, S. S.** (1985). Optical torque exerted on a homogeneous sphere levitated in the circularly polarized fundamental-mode laser beam, *JOSA B*, *2*(11), 1853–1860.

[**69**] **Gouesbet, G., Grehan, G., & Maheu, B.** (1990). Localized interpretation to compute all the coefficients gnm in the generalized Lorenz–Mie theory, *JOSA A*, *7*(6), 998–1007.

[**70**] **Lock, J. A.** (1995). Improved Gaussian beam-scattering algorithm, *Applied Optics*, *34*(3), 559–570.

[**71**] **Maheu, B., Gréhan, G., & Gouesbet, G.** (1989). Ray localization in Gaussian beams, *Optics Communications*, *70*(4), 259–262.

[**72**] **Lock, J. A.** (1993). Contribution of high-order rainbows to the scattering of a Gaussian laser beam by a spherical particle, *JOSA A*, *10*(4), 693–706.

[**73**] **Lock, J. A., & Gouesbet, G.** (1994). Rigorous justification of the localized approximation to the beam-shape coefficients in generalized Lorenz–Mie theory. I. On-axis beams, *JOSA A*, *11*(9), 2503–2515.

[**74**] **Lock, J. A., & Gouesbet, G.** (1994). Rigorous justification of the localized approximation to the beam-shape coefficients in generalized Lorenz–Mie theory. II. Off-axis beams, *Journal of the Optical Society of America A*, *11*(9), 2516–2525. https://doi.org/10.1364/JOSAA.11.002516

[**75**] **Lock, J. A.** (2006). Partial-wave expansions of angular spectra of plane waves, *JOSA A*, *23*(11), 2803–2809.

[**76**] **Gouesbet, G.** (1999). Validity of the localized approximation for arbitrary shaped beams in the generalized Lorenz–Mie theory for spheres, *JOSA A*, *16*(7), 1641–1650.

[**77**] **Gouesbet, G., Lock, J. A., & Gréhan, G.** (1995). Partial-wave representations of laser beams for use in light-scattering calculations, *Applied Optics*, *34*(12), 2133–2143.

[**78**] **Lock, J. A.** (2004). Calculation of the radiation trapping force for laser tweezers by use of generalized Lorenz-Mie theory. II. On-axis trapping force, *Applied Optics*, *43*(12), 2545–2554.

[**79**] **Lock, J. A.** (2004). Calculation of the radiation trapping force for laser tweezers by use of generalized Lorenz-Mie theory. I. Localized model description of an on-axis tightly focused laser beam with spherical aberration, *Applied Optics*, *43*(12), 2532–2544.

[**80**] **Ren, K. F., Gouesbet, G., & Gréhan, G.** (1998). Integral localized

approximation in generalized Lorenz–Mie theory, *Applied Optics*, *37*(19), 4218–4225.

[**81**] **Gouesbet, G.** (1999). Validity of the cylindrical localized approximation for arbitrary shaped beams in generalized Lorenz-Mie theory for circular cylinders, *Journal of Modern Optics*, *46*(8), 1185–1200. https://doi.org/10.1080/09500349908231329

[**82**] **Gouesbet, G., & Mees, L.** (1999). Validity of the elliptical cylinder localized approximation for arbitrary shaped beams in generalized Lorenz–Mie theory for elliptical cylinders, *JOSA A*, *16*(12), 2946–2958.

[**83**] **Polaert, H., Gouesbet, G., & Gréhan, G.** (1998). Measurement of beam-shape coefficients in the generalized Lorenz–Mie theory for the on-axis case, *Applied Optics*, *37*(21), 5005–5013.

[**84**] **Polaert, H., Gouesbet, G., & Gréhan, G.** (2001). Laboratory determination of beam-shape coefficients for use in generalized Lorenz–Mie theory, *Applied Optics*, *40*(10), 1699–1706.

[**85**] **Ren, K. F., Gréhan, G., & Gouesbet, G.** (1996). Prediction of reverse radiation pressure by generalized Lorenz–Mie theory, *Applied Optics*, *35*(15), 2702–2710. https://doi.org/10.1364/AO.35.002702

[**86**] **Ren, K. F., Grehan, G., & Gouesbet, G.** (1994). Radiation pressure forces exerted on a particle arbitrarily located in a Gaussian beam by using the generalized Lorenz-Mie theory, and associated resonance effects, *Optics Communications*, *108*(4–6), 343–354.

[**87**] **Camenzind, K.** (2013). *Quantifying Trapping Forces in a Simplified Optical Tweezers Setup*. California.

[**88**] **Keen, S., Leach, J., Gibson, G., & Padgett, M. J.** (2007). Comparison of a high-speed camera and a quadrant detector for measuring displacements in optical tweezers, *Journal of Optics A: Pure and Applied Optics*, *9*(8), S264.

[**89**] **Otto, O., Gutsche, C., Kremer, F., & Keyser, U. F.** (2008). Optical tweezers with 2.5 kHz bandwidth video detection for single-colloid electrophoresis, *Review of Scientific Instruments*, *79*(2), 23710.

[**90**] **Gibson, G. M., Leach, J., Keen, S., Wright, A. J., & Padgett, M. J.** (2008). Measuring the accuracy of particle position and force in optical tweezers using high-speed video microscopy, *Optics Express*, *16*(19), 14561–14570.

[**91**] **Gong, Z., Chen, H., Xu, S., Li, Y., & Lou, L.** (2006). Monte-Carlo simulation of optical trap stiffness measurement, *Optics Communications*, *263*(2), 229–234.

[**92**] **Visscher, K., Gross, S. P., & Block, S. M.** (1996). Construction of multiple-beam optical traps with nanometer-resolution position sensing, *IEEE Journal of Selected Topics in Quantum Electronics*, *2*(4), 1066–1076.

[**93**] **Simmons, R. M., Finer, J. T., Chu, S., & Spudich, J. A.** (1996). Quantitative measurements of force and displacement using an optical trap, *Biophysical Journal*, *70*(4), 1813–1822.

[**94**] **Neuman, K. C., & Block, S. M.** (2004). Optical trapping, *Review of Scientific Instruments*, *75*(9), 2787–2809.

[**95**] **Smith, S. P.** (1999). Inexpensive optical tweezers for undergraduate laboratories, *American Journal of Physics*, *67*(1), 26. https://doi.org/10.1119/1.19187

[**96**] **Griot, M.** (2009). Gaussian beam optics,. Retrieved November 4, 2017, from

http://www.mellesgriot.com

[**97**] **Alda, J.** (2003). Laser and Gaussian beam propagation and transformation, *Encyclopedia of Optical Engineering, 2013*, 999–1013.

[**98**] Gaussain Beam Optics, (n.d.). Retrieved October 20, 2017, from https://www.newport.com/n/gaussian-beam-optics

[**99**] **Lei, C. T.** (2005). Gaussian Beam,. Colorado. Retrieved from https://www.colorado.edu/physics/phys4510/phys4510_fa05/Chapter5.pdf

[**100**] **Peatross, J., & Ware, P.** (2015). *Physics of Light and Optics*. https://doi.org/10.1364/FIO.2010.JWA64

[**101**] **Stace, C.** (n.d.) Using ABCD Matrices to find the position of a Gaussian beam waist,. Bristol: LumOptica.

[**102**] **Jia, D., Hamilton, J., Zaman, L. M., & Goonewardene, A.** (2007). The time, size, viscosity, and temperature dependence of the Brownian motion of polystyrene microspheres, *American Journal of Physics*, *75*(2), 111–115.

[**103**] **Schindelin, J., Arganda-Carreras, I., Frise, E., Kaynig, V., Longair, M., Pietzsch, T., … Schmid, B.** (2012). Fiji: an open-source platform for biological-image analysis, *Nature Methods*, *9*(7), 676–682.

[**104**] **Ertugay, M. F., Baslar, M., Sengul, M., & Sallan, S.** (2012). The effect of acoustic energy on viscosity and serum separation of traditional ayran, a Turkish yogurt drink, *Gida*, *37*, 253–257.

[**105**] Gıda Maddeleriyle İlgili Tüzük ve Yürürlülük, Pub. L. No. 55 (1998). Turkey: İstanbul Ticaret Odası.

[**106**] **Torres, J. D., Tárrega, A., & Costell, E.** (2010). Storage stability of starch-based dairy desserts containing long-chain inulin: Rheology and particle size distribution, *International Dairy Journal*, *20*(1), 46–52. https://doi.org/https://doi.org/10.1016/j.idairyj.2009.08.001

[**107**] **Rappaz, B., Charrière, F., Depeursinge, C., Magistretti, P. J., & Marquet, P.** (2008). Simultaneous cell morphometry and refractive index measurement with dual-wavelength digital holographic microscopy and dye-enhanced dispersion of perfusion medium, *Opt. Lett.*, *33*(7), 744–746. https://doi.org/10.1364/OL.33.000744

APPENDICES

APPENDIX A: ABCD MATLAB CODES FOR GAUSSIAN BEAM PROPAGATION

```
%Codes were written by Kristoffer Lemoins and modified from Dr. Alan Cheville
%=====================================================

%Waist Radius and Radius of Curvature Calculation After Telescope System
f1=input('enter the the focal length f1 in mm:')/1000 %input focal length f1
f2=input('enter the the focal length f2 in mm:')/1000 %input focal length f2
d1=f1+f2; %distance of telescope is sum of focal lengths
wo=input('enter the the initial waist radius in mm:')/1000; %input waist radius
x=input('enter the distance that you would like to track the output beam in m:');

lamda=632.8e-9 % He-Ne lasers wavelength

%At first set up the matrices for lens 1, lens 2, space between lenses and space after
lenses by using capital letters for matrices.

L1=[1 0;-1/f1 1];
L2=[1 0;-1/f2 1];
D1=[1 d1;0 1];

Ro=1e60; %R is essentially infinity, but Matlab can't handle infinity..

%now calculate starting q
qo=(1/Ro-j*lamda/(pi*wo^2))^(-1);

%Now loop through distances, plotting w(z) and R(z) at each point
N=500;
D2=linspace(0,x,N); %define d2 as a user-specified distance

for k=1:N
    %find D2 for a given distance
    D2=[1 d2(k);0 1];

    %ABCD matrix of the system − multiply in reverse order.
    M=D2*L2*D1*L1;

    %Now figure out R(d2) and w(d2) using formula to calculate 1/q
    %first find A, B, C, D
```

```matlab
    A=M(1,1);B=M(1,2);C=M(2,1);D=M(2,2);
    %Now get 1/q
    oneoverq=(C+D/qo)/(A+B/qo);
    %Get R(d2) from real part
    R(k)=(real(oneoverq))^(-1);
    %w(d2) from imaginary part
    oneoverqi=-imag(oneoverq);
    w(k)=sqrt(lamda/pi(oneoverqi));
end

%Now plot up results.
subplot(2,1,1);
semilogy(d2,w*1000)
xlabel('Distance after telescope (m)')
ylabel('Waist Radius (mm)')
title('Waist Radius After Telescope System')
grid on;
subplot(2,1,2);
semilogy(d2,R);
grid on;
xlabel('Distance after telescope (m)')
ylabel('Radius of Curvature (m)')
title('Radius of Curvature After Telescope System')

%===================================================
%Calculations after Lens 5
f1=input('enter the the focal length f1 in mm:')/1000 %input focal length f1
f2=input('enter the the focal length f2 in mm:')/1000 %input focal length f2
d12=f1+f2; %distance of telescope is sum of focal lengths
f5=input('enter the the focal length f5 in mm:')/1000; %input focal length f5
d25= input('enter the distance between lens 2 and lens 3 in mm:')/1000;
wo=input('enter the the initial waist radius in mm:')/1000; %input waist radius
x=input('enter the distance that you would like to track the output beam in m:');
lamda=632.8e-9 % He-Ne lasers wavelength

%At first set up the matrices for lens 1, lens 2,  lens 5, space between lenses and
space after lenses by using capital letters for matrices.

L1=[1 0;-1/f1 1];
L2=[1 0;-1/f2 1];
L5=[1 0;-1/f5 1];
D12=[1 d12;0 1];
D25=[1 d25;0 1];

Ro=1e60; %R is essentially infinity, but Matlab can't handle infinity..

%now calculate starting q
qo=(1/Ro-j*lamda/(pi*wo^2))^(-1);
```

```matlab
%Now loop through distances, plotting w(z) and R(z) at each point
N=500;
d5=linspace(0,x,N); %define d5 as a user-specified distance

for k=1:N
    %find D5 for a given distance
    D5=[1 d5(k);0 1];

    %ABCD matrix of the system – multiply in reverse order.
    M=D5*L5*D25*L2*D12*L1;

    %Now figure out R(d5) and w(d5) using formula to calculate 1/q
    %first find A, B, C, D
    A=M(1,1);B=M(1,2);C=M(2,1);D=M(2,2);
    %Now get 1/q
    oneoverq=(C+D/qo)/(A+B/qo);
    %Get R(d5) from real part
    R(k)=(real(oneoverq))^(-1);
    %w(d5) from imaginary part
    oneoverqi=-imag(oneoverq);
    w(k)=sqrt(lamda/pi(oneoverqi));
end
subplot(2,1,1);
semilogy(d5,w*1000);
hold on;
wobj=2.5;
plot(d5,wobj*ones(size(d5)));
hold off
xlabel('Distance after Lens 5 (m)');
ylabel('Waist Radius (mm)');
title('Waist Radius After Optical System');
grid on
subplot(2,1,2);
plot(d5,R*1000);
hold on;
robj=140;
plot(d5,robj*ones(size(d5)));
hold off;
xlabel('Distance after Lens 5 (m)');
ylabel('Radius of Curvature (mm)');
title('Radius of Curvature After Optical System');
grid on
y=min(w*1000); % This is the minimum waist size of the beam in mm

%====================================================
%Calculations after objective
```

```
f1=input('enter the the focal length f1 in mm:')/1000 %input focal length f1
f2=input('enter the the focal length f2 in mm:')/1000 %input focal length f2
d12=f1+f2; %distance of telescope is sum of focal lengths
f5=input('enter the the focal length f5 in mm:')/1000; %input focal length f5
d25= input('enter the distance between lens 2 and lens 5 in mm:')/1000;
d5O= input('enter the distance between lens 5 and the objective in mm:')/1000;
wo=input('enter the the initial waist radius in mm:')/1000; %input waist radius
fo=1.8 %focal length of objective – Edmund optics
wo=fo; %working distance of objective – plot is useless beyond this distance
lamda=632.8e-9 % He-Ne lasers wavelength

%At first set up the matrices for lens 1, lens 2, lens 5, the objective, space between
lenses and space after lenses by using capital letters for matrices.

L1=[1 0;-1/f1 1];
L2=[1 0;-1/f2 1];
L5=[1 0;-1/f5 1];
LO=[1 0;-1/fo 1];
D12=[1 d12;0 1];
D25=[1 d25;0 1];
D5O=[1 d5O;0 1];

Ro=1e60; %R is essentially infinity, but Matlab can't handle infinity..

%now calculate starting q
qo=(1/Ro-j*lamda/(pi*wo^2))^(-1);

%Now loop through distances, plotting w(z) and R(z) at each point
N=500;
dOb=linspace(0,x,N); %define dOb as a user-specified distance

for k=1:N
    %find D5 for a given distance
    DOb=[1 dOb(k);0 1];

    %ABCD matrix of the system – multiply in reverse order.
    M=DOb*LO*D5O*L5*D25*L2*D12*L1;

    %Now figure out R(dOb) and w(dOb) using formula to calculate 1/q
    %first find A, B, C, D
    A=M(1,1);B=M(1,2);C=M(2,1);D=M(2,2);
    %Now get 1/q
    oneoverq=(C+D/qo)/(A+B/qo);
    %Get R(dOb) from real part
    R(k)=(real(oneoverq))^(-1);
    %w(dOb) from imaginary part
    oneoverqi=-imag(oneoverq);
    w(k)=sqrt(lamda/pi(oneoverqi));
```

```
end
subplot(2,1,1);
semilogy(d5,w*1000*1000/100); %plot in um and compensate for 100X of objective
xlabel('Distance after Objective (m)');
ylabel('Waist Radius (um)');
title('Waist Radius After Optical System');
grid on
subplot(2,1,2);
plot(d5,R*1000*1000/100); %convert to um and compensate for 100X of objective
xlabel('Distance after Objective (m)');
ylabel('Radius of Curvature (um)');
title('Radius of Curvature After Optical System');
grid on
```

CURRICULUM VITAE

Name Surname	**: Nur Çobanoğlu**
Place and Date of Birth	**: İzmir / 7th of October, 1993**
E-Mail	**: ncobanoglu93@gmail.com**

EDUCATION **:**

- **B.Sc.** **:** 2016, Ege University, Faculty of Engineering, Department of Mechanical Engineering

List of Publications:

Conference Paper

Book Chapter